Ocean-only FAFMIP: Understanding Regional Patterns of Ocean Heat Content and Dynamic Sea Level Change.

Alexander Todd[1], Laure Zanna[2,1], Matthew Couldrey[3], Jonathan Gregory[3,4], Quran Wu[3], John Church[5], Riccardo Farneti[6], René Navarro-Labastida[6,7], Kewei Lyu[8], Oleg Saenko[9], Duo Yang[9], Xuebin Zhang[8]

[1]Department of Physics, University of Oxford, Oxford, UK
[2]New York University Courant Institute, New York, NY, USA
[3]National Centre for Atmospheric Science, University of Reading, Reading, UK
[4]Met Office Hadley Centre, Exeter, UK
[5]Climate Change Research Centre, University of New South Wales, Sydney, New South Wales, Australia
[6]Earth System Physics, Abdus Salam International Centre for Theoretical Physics, Trieste, Italy
[7]ESFM Doctorate School, Università degli Studi di Trieste, Italy
[8]Centre for Southern Hemisphere Oceans Research (CSHOR), CSIRO Oceans and Atmosphere, Hobart, Tasmania, Australia
[9]Canadian Centre for Climate Modelling and Analysis, Canada

Key Points:

- Dynamic sea level change spread is large in response to model-independent surface heat flux change.
- Ocean circulation sensitivity modulates the dynamic sea level change in the North Atlantic.
- Ocean circulation weakening is amplified by an atmospheric feedback in coupled climate models.

Corresponding author: Alexander Todd, `alexander.todd@physics.ox.ac.uk`

Abstract

There is large uncertainty in the future sea level change at regional scales under anthropogenic global warming. This study uses a novel design of ocean-only general circulation model (OGCM) experiments to investigate the ocean's response to surface buoyancy and momentum flux perturbations, as part of the Flux-Anomaly-Forced Model Intercomparison Project (FAFMIP), and compares with results from coupled, atmosphere-ocean GCM (AOGCM) experiments. Much of the inter-model spread is driven by the response to surface heat flux perturbations. In a multi-model ensemble of OGCMs forced with identical surface heat flux perturbations, regional sea level and ocean heat content changes demonstrate considerable disagreement, especially in the North Atlantic. Spread in both residual mean advection and diapycnal diffusion changes contribute to much of the multi-model disagreement over regional heat content change. Residual mean advection changes are related to the large spread in simulated Atlantic meridional overturning circulation (AMOC) weakening (20-50%). We find approximately 10% more AMOC weakening in response to surface heat flux perturbations in AOGCMs relative to OGCMs with consistent ocean models. This enhanced AMOC weakening is driven by an atmosphere-ocean feedback which amplifies the surface heat flux perturbation. In the North Pacific, there is little agreement amongst the ensemble over which processes lead to ocean warming, with varying contributions from residual mean advection and diapycnal diffusion. For the Pacific basin, the atmosphere-ocean feedback reduces sea surface temperature (SST) warming by 0.5°C. In the Southern Ocean, the atmosphere-ocean feedback is not generally important for buoyancy and momentum flux perturbations.

Plain Language Summary

A rise in sea level, as a result of climate change due to human activity, is a major threat to coastal communities and environments. Sea level rise is partially caused by a warming and expansion of the world's oceans, due to a net heat input from the atmosphere to the ocean. Changes in rainfall patterns and surface winds also affect the sea level, but net heat input changes are the most important factor. State-of-the-art computer models disagree on future projections of local sea level rise. It has been suggested that this disagreement comes from differences in the amount of net heat input, and also the different assumptions going into the computer models. We find a large local sea level rise disagreement in the North Atlantic from giving several different computer models the same net heat input change. These differences are linked to uncertainty in how much Atlantic currents will slow in response to a given amount of warming. We also find that computer models which include both atmosphere and ocean components slow the Atlantic currents by more than computer models with just an ocean. This finding builds our knowledge of the processes which determine the ocean's role in climate change.

1 Introduction

A rise in global mean sea level is a robust feature of projected anthropogenic climate change from state-of-the-art atmosphere-ocean general circulation models (AOGCMs) (Church et al., 2013; Slangen et al., 2014). Simulated global mean sea level rise is largely due to a net ocean heat uptake, leading to thermal expansion, and total ocean mass increase due to reduced terrestrial water and ice storage (Church et al., 2013). However, there is considerable disagreement amongst AOGCMs contributing to the Coupled Model Intercomparison Project, phase 5 (CMIP5, (Taylor et al., 2012)) on the more policy-relevant regional patterns of sea level change (Yin, 2012; Bouttes et al., 2012; Church et al., 2013; Bouttes & Gregory, 2014). Air-sea buoyancy and momentum flux changes are coupled to ocean dynamic and thermodynamic changes, and play an important role in modulating regional sea level change (Lowe & Gregory, 2006; Bouttes & Gregory, 2014).

Dynamic sea level (DSL) change is a useful metric for examining the processes which modulate regional sea level. DSL is defined as $\zeta = \eta - \bar{\eta}$, where η is the sea surface height relative to a fixed geopotential surface, and $\bar{\cdot}$ represents a global mean. Hence, DSL change, $\Delta\zeta = \Delta\eta - \Delta\bar{\eta}$, has a global mean equal to zero by construction. Changes in depth integrated ocean circulation directly contribute to $\Delta\zeta$ via a barotropic component. Circulation change is also strongly coupled to temperature and salinity changes, which affects density, and contributes to $\Delta\zeta$ through a baroclinic component. Typically, at mid and high latitudes, the baroclinic component of $\Delta\zeta$ has a much larger magnitude than the barotropic component (Lowe & Gregory, 2006).

Coupled AOGCMs generally simulate qualitatively consistent $\Delta\zeta$ responses to greenhouse gas forcing in three regions. Reduced heat loss and increased precipitation over the high latitude North Atlantic inputs buoyancy, weakens the Atlantic meridional overturning circulation (AMOC) and leads to a meridional $\Delta\zeta$ dipole. This $\Delta\zeta$ dipole is characterised by relative sea level increases and decreases over the subpolar and subtropical gyres, respectively (Bouttes et al., 2013). Over the North Pacific, an opposite $\Delta\zeta$ dipole is simulated, due to relatively enhanced heat uptake over the subtropical gyre, and increased zonal wind stress which accelerates the gyre circulation (Yin et al., 2010). In the Southern Ocean, a similar $\Delta\zeta$ dipole is evident, with relative sea level increases and decreases north and south of the Antarctic Circumpolar Current (ACC), respectively. Increased buoyancy input at high Southern Ocean latitudes is advected northwards via Ekman transport. This Ekman transport of relatively low density water is further enhanced due to increased westerly wind stress over the ACC, leading to the meridional DSL change dipole (Lowe & Gregory, 2006; Bouttes et al., 2012; Marshall et al., 2015; Saenko et al., 2015). The North Pacific and Southern Ocean features are common in a majority of models, with weaker consensus for the North Atlantic (Slangen et al., 2014). There is little consensus on the rate at which regional anthropogenic $\Delta\zeta$ will emerge from natural variability due to disagreement in the unperturbed and forced inter-annual variability, and uncertainty in the sensitivity of ocean dynamics to surface forcing (Lyu et al., 2014).

In order to investigate the spread in DSL projections under greenhouse gas forcing, Gregory et al. (2016) devised the Flux-Anomaly-Forced Model Intercomparison Project (FAFMIP), a novel set of AOGCM experiments and diagnostics to contribute towards CMIP phase 6 (CMIP6). Part of the spread in DSL projections from AOGCMs arises from the global and local ocean dynamical and thermodynamical response to greenhouse gas forcing, leading to different patterns of surface flux changes (Bouttes et al., 2012). The FAFMIP experiments involve prescribing time-independent (except for a seasonal cycle) surface buoyancy and momentum flux perturbations (presented in Figure 1 and discussed further in Section 2) to an ensemble of several different AOGCMs. The perturbations are the same in all models, so this framework estimates the model response driven spread in DSL change uncertainty. A further experiment involves applying the buoyancy and momentum flux perturbations simultaneously. Comparing the response to this simultaneous perturbation with the sum of the responses to the individual perturbations, the nonlinear response to heat, freshwater and momentum flux changes can also be diagnosed.

This study presents an ocean-only FAFMIP investigation, building and complementing the AOGCM analysis of Gregory et al. (2016). Here we use an ensemble of five ocean general circulation models (OGCMs), and two AOGCMs with ocean components from the OGCM ensemble. Two aims motivate this study of the ocean's role in future DSL change:

The first aim is the one which motivates FAFMIP, namely to examine how much of the spread in regional patterns of $\Delta\zeta$ and heat content change in coupled AOGCMs is due to the use of different ocean models. Individual OGCMs simulate a range of background states, use a variety of spatial grids and incorporate different sub-grid scale parametrisations, with varying biases relative to the observed ocean state (Flato et al., 2013). The ocean-only FAFMIP extends the comparison by including models which are not used in CMIP5.

The second aim of this study is to quantify the effect of atmosphere feedbacks on ocean climate change. In ocean-only FAFMIP experiments, no surface restoring or bulk formulae for ocean-atmopshere coupling is applied in the forced scenarios. In coupled FAFMIP experiments, the atmosphere responds to changes in sea-surface conditions simulated by the ocean, producing a coupled feedback. For example, the applied heat flux perturbation induces a weakening of the Atlantic Meridional Overturning Circulation, leading to a cooling in the North Atlantic, and hence an increase in the heat flux into the ocean, as a positive feedback.By comparing AOGCM and OGCM simulations performed with an identical ocean model, this and other such coupled feedbacks can be quantified, because they do not occur in the ocean-only FAFMIP experiments.

The OGCM and AOGCM FAFMIP methods are described in Section 2. Section 3 presents an analysis of the ocean circulation, heat content and DSL change in the surface heat flux perturbation experiment, FAF-heat. Section 4 extends this analysis to the surface freshwater (FAF-water) and momentum (FAF-stress) flux perturbation experiments, in addition to the simultaneous surface flux perturbation experiment (FAF-all). Finally, Section 5 presents the conclusions.

2 Methods

Five ocean general circulation models (OGCMs: MITgcm, MOM5, ACCESS-OM2, HadOM3 and NEMO3.4) and two coupled, atmosphere-ocean general circulation models (AOGCMs: HadCM3 and CanESM5) are used in this study. Model acronyms, forcing data and technical details are presented in Table 1. HadOM3 and NEMO3.4 are the ocean components to HadCM3 and CanESM5, respectively. MOM5 and ACCESS-OM2 are two slightly different configurations of the NOAA-GFDL Modular Ocean Model, version 5 (S. Griffies, 2012). Initial conditions for MOM5 and ACCESS-OM2 are from the end of a 4000 year spin up with prescribed COREv2 forcing data (Large & Yeager, 2009), and the end of a 1000 year spin up with prescribed JRA55-do normal year forcing data (Tsujino et al., 2018), respectively. Hence, intercomparison between MOM5 and ACCESS-OM2 provides an estimate of the effect of using different background ocean states.

Amongst the OGCM ensemble, the horizontal grid resolution is nominally between 2.8° to 1° latitude $\times$ longitude, with vertical grids using between 15 to 50 irregularly spaced levels, with level thickness increasing with depth. All OGCMs use the Gent and McWilliams (1990) (GM) eddy parametrisation scheme to represent sub-grid, mesoscale eddies. MITgcm, MOM5, ACCESS-OM2 and HadOM3 implement a skew-flux closure (S. M. Griffies, 1998) of the GM scheme, with MITgcm, HadOM3 and NEMO3.4 using the Visbeck et al. (1997) scheme to estimate the isopycnal diffusion coefficient from the diagnosed Eady growth rate. There is no sea-ice model active in any of the OGCMs, whereas both AOGCMs include a thermodynamic-dynamic sea-ice model. Further details of the parametrisations used in each model are presented in Appendix A.

To produce statistically equilibrated initial conditions, the OGCMs except for HadOM3 are integrated for several thousand years with either a prescribed monthly climatology (MITgcm) or daily varying (ACCESS-OM2 and NEMO3.4) air-sea heat, Q in W m^{-2}, freshwater, W in kg m^{-2} s^{-1}, and momentum fluxes, τ in Pa, or a prescribed atmospheric climatological state from which these fluxes are estimated via bulk formulae (MOM5). The MITgcm and NEMO3.4 surface conditions are derived from a AOGCM pre-industrial simulations, with the ACCESS-OM2 and MOM5 surface conditions representative of late twentieth century observations. Following Huber and Zanna (2017), in MITgcm the surface layer is relaxed to climatologies of sea surface temperature (θ^*) and sea surface salinity (S^*) on time scales of 60 and 90 days, respectively. A similar restoration of SST and SSS in NEMO3.4 and ACCESS-OM2 is also applied (Table 1). For the coupled AOGCMs (HadCM3 and CanESM5) initial conditions are obtained from a long running spin up simulation with prescribed pre-industrial control greenhouse gas concentrations and aerosol forcing. By definition, the HadOM3 initial conditions are identical to HadCM3.

The FAF-control simulation for HadCM3 and CanESM5 is performed by continuing the spin up simulation for a further 70 years. For HadOM3, daily atmosphere-ocean and sea ice-ocean buoyancy and momentum fluxes from the HadCM3 FAF-control simulation are prescribed directly to the HadCM3 ocean component with no atmospheric coupling. Hence, the HadOM3 and HadCM3 FAF-control simulations are identical. For the other OGCMs, the spin up simulations are also continued for a further 70 years in order to produced restored control simulations. In these restored control simulations, the effective air-sea heat and freshwater fluxes from the prescribed surface restoration are diagnosed and saved at 6-hourly (ACCESS-OM2, NEMO3.4) or daily (MITgcm, MOM5) intervals. Here, surface restoration refers to either the θ^* and S^* relaxation plus prescribed buoyancy fluxes applied in ACCESS-OM2, MITgcm and NEMO3.4, or the use of bulk formulae with a fixed atmospheric state in MOM5. Consider temperature, θ, and salinity, S, in the surface layer for MITgcm. Advection and diffusion are governed by:

$$\frac{\partial \theta}{\partial t} + (\mathbf{u} \cdot \nabla)\theta - \nabla \cdot (\kappa \nabla \theta) = -\lambda_\theta(\theta - \theta^*) + \frac{Q}{\rho_0 c_p \Delta z_s}, \tag{1}$$

and

$$\frac{\partial S}{\partial t} + (\mathbf{u} \cdot \nabla)S - \nabla \cdot (\kappa \nabla S) = -\lambda_S(S - S^*) - \frac{S_0 W}{\rho_0 \Delta z_s}, \tag{2}$$

where ∇ is the three-dimensional (3-D) gradient operator, $\mathbf{u}$ is the 3-D resolved velocity vector, κ represents the 3-D diffusivity coefficient, λ_θ and λ_S are the reciprocals of the temperature and salinity restoration timescales, in s^{-1}, respectively, $\rho_0 = 1035$ kg m^{-3}, $S_0 = 35$ psu, $c_p = 4000$ J K^{-1} kg^{-1} are the reference density, salinity and specific heat capacity values, and $\Delta z_s = 50$m is the thickness of the surface layer. In this example, $-\lambda_\theta(\theta-\theta^*) - \frac{Q}{\rho_0 c_p \Delta z_s}$ and $-\lambda_S(S-S^*) - \frac{S_0 F}{\Delta z_s}$ are diagnosed as the effective air-sea heat and freshwater fluxes, respectively. In the surface layer, the momentum balance is given by

$$\frac{\partial \mathbf{u}}{\partial t} + (\mathbf{u} \cdot \nabla)\mathbf{u} + \frac{1}{\rho}\nabla p - \mathbf{f} \times \mathbf{u} - \nabla \cdot (\kappa \nabla \mathbf{u}) = \frac{\tau}{\rho_0 \Delta z_s}, \tag{3}$$

where p is the pressure and $\mathbf{f}$ is the Coriolis vector. In the restored control period is re-run with the control momentum and effective surface buoyancy forcing, without any surface restoration. These buoyancy and momentum flux-only runs form the FAF-control simulations for ACCESS-OM2, MITgcm, MOM5, and NEMO3.4. In all cases, using high temporal frequency forcing fluxes is essential to the FAF-control design in order to minimise any drift away from the spin up control climate (as in Method C of Gregory et al. (2016)). Note that FAF-control uses flux forcing alone, without any surface restoration, since the aim is to eliminate any processes which would cause surface fluxes to react to the surface state (as in Method B of Gregory et al. (2016)).

Four perturbation experiments are performed: FAF-heat, FAF-water, FAF-stress and FAF-all, closely following the protocol presented by Gregory et al. (2016). In FAF-heat, FAF-water and FAF-stress, a constant (except for a seasonal cycle) surface heat (Q'), freshwater (W') and momentum (τ') flux perturbation is applied, respectively. In FAF-all, all three perturbations are applied simultaneously. These flux perturbations are calculated from the twelve month climatological CMIP5 ensemble mean difference between years 61-80 of the 1% CO_2 year^{-1} simulation and all years of the pre-industrial control simulation, and bilinearly interpolated onto each model's native grid. Figure 1 shows the annual mean of the FAFMIP surface perturbations. In order to restrict excessive ocean cooling, negative Q' over the Barents and Kara sea regions (ocean grid points between 15°E-135°E and north of 60°N) are reset to zero. This has the effect of adding

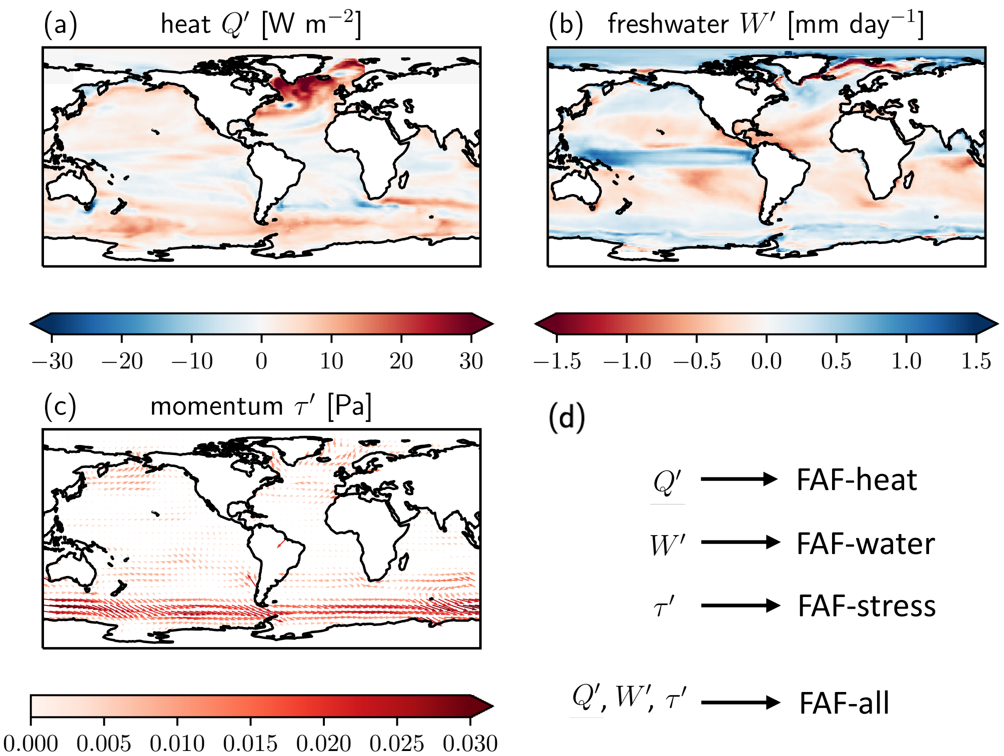

Figure 1. FAFMIP annual mean surface flux perturbations. Colours in (a) and (b) show the surface heat (FAF-heat) and surface freshwater (FAF-water) flux perturbations, respectively. Note that the surface heat flux perturbation over the Barents and Kara seas is reset to zero. In (c), colours indicate the magnitude, and arrows the direction, of the surface momentum flux perturbation (FAF-stress). All flux perturbations are defined as positive downwards, from the atmosphere to the ocean. In (d), a schematic demonstrates the surface flux perturbations applied in each experiment.

approximately 3% to the globally integrated atmosphere to ocean heat flux perturbation relative to the original FAF-heat Q' presented by Gregory et al. (2016). Since this difference is small relative to the global mean FAF-heat perturbation (1.8 W m^{-2}), we continue to refer to the present heat flux perturbation experiment as FAF-heat. Since the OGCMs do not include a sea ice component, any of the perturbation experiments could lead to changes in ocean circulation and heat convergence which might result in SST below freezing. However, this effect is typically found to be small and localised, with further detail provided in Appendix Appendix A.

A similar ocean-only experimental design has previously been implemented by Marshall et al. (2015) and Zika et al. (2018). Marshall et al. (2015) included a feedback to damp SST change. This is not done in ocean-only FAFMIP experiments because we specifically wish to avoid surface flux feedbacks on ocean climate change, as it would interfere strongly with the imposed heat flux perturbation. Zika et al. (2018) used a repeating 10 year climatology of effective surface fluxes, in contrast to the entire 70 year period of effective surface fluxes considered in this study. Moreover, Zika et al. (2018) considered more idealised surface flux perturbations relative to FAFMIP, including a global amplification of the freshwater flux and globally uniform surface heat flux change.

The AOGCM FAF-heat simulations for HadCM3 and CanESM5 are performed following method B of the FAFMIP protocol (Bouttes & Gregory, 2014; Gregory et al., 2016). In the respective ocean components, a redistributed passive temperature tracer is introduced, θ_R, initialised everywhere at the control temperature at the end of the spin up simulation. θ_R only experiences the unperturbed atmosphere to ocean heat flux, Q. An added passive temperature tracer, θ_A, initialised at 0 everywhere and experiencing only Q', is also introduced. The surface layer of θ_R is the sea surface temperature used by the atmosphere to compute Q. Meanwhile, the active temperature field, θ, experiences $Q+Q'$, and hence stratification, circulation and heat content can change. The FAF-water and FAF-stress simulations are performed by directly perturbing the atmosphere-ocean freshwater and momentum fluxes, respectively, since the atmosphere feedback to these perturbations is fairly small.

The OGCM FAF-heat simulations for ACCESS-OM2, MITgcm, MOM5 and NEMO3.4 are performed by directly applying Q' to the respective FAF-control atmosphere-ocean heat fluxes. For the HadOM3 FAF-heat simulation, Q' is applied to the FAF-control atmosphere-ocean and sea ice-ocean heat fluxes in open ocean and sea ice covered regions, respectively. This HadOM3 approach is slightly different from the method C protocol described by Gregory et al. (2016). Under method C, the sea ice model interacts with the redistributed SST, which may lead to a change in the sea ice-ocean buoyancy fluxes relative to FAF-control. In addition, the method C protocol suggested using a monthly climatology which produced a substantial drift in the ocean state. By using higher frequency surface forcing in this study, the drift is negligible. Similar to the AOGCM experiments, an added passive temperature tracer, θ_A, is also introduced in OGCMs. The redistributed temperature change can then be computed off-line as the difference $\theta - \theta_A$. The corresponding FAF-water and FAF-stress simulations are performed by directly applying W' and τ' to the FAF-control freshwater and momentum fluxes, respectively.

Annual mean temperature, salinity, velocity and dynamic sea level diagnostics for each simulation are saved on each model's native grid. In addition, temperature and salinity tendency diagnostics, as presented in Table 4 of Gregory et al. (2016), are saved as annual means. Kuhlbrodt et al. (2015) review the use of temperature tendency diagnostics in previous studies, demonstrating that global mean ocean heat content change is largely a balance of downward advection changes in the extratropics, compensated by upward isopycnal diffusion changes, mainly in the Southern Ocean. In the following analysis, regional, basin and global means are computed on each model's native grid. For spatial intercomparisons, all model data is bilinearly interpolated onto the MITgcm regular 2.8° latitude × longitude grid.

3 FAF-heat Intercomparison

This section examines the OGCM and AOGCM responses in the FAF-heat simulation. Discussion of ocean heat content and dynamic sea level change focuses on the mean difference between FAF-heat and FAF-control during the last decade, year 61-70, of each experiment.

3.1 Ocean Circulation

Amongst the OGCM and AOGCM ensemble, the 70 year mean FAF-control Atlantic meridional overturning circulation (AMOC) strength, Ψ_{AMOC}, varies between 11-21 Sv (1 Sv $\equiv 10^6$ m^3 s^{-1}). Here, Ψ_{AMOC} is defined as the maximum of the overturning streamfunction between 20°N and 60°N, and beneath 500 m depth (Huber & Zanna, 2017). This spread in mean AMOC strength is consistent with the CMIP5 multi-model ensemble pre-industrial control simulations (Wang et al., 2014). Huber and Zanna (2017) found that spread in AMOC strength amongst CMIP5 models is dominated by differences in high latitude surface heat fluxes. The relative FAF-heat AMOC strength change, $\Delta\Psi_{AMOC}$, over time is presented in Figure 2(a). The rate of AMOC weakening in FAF-

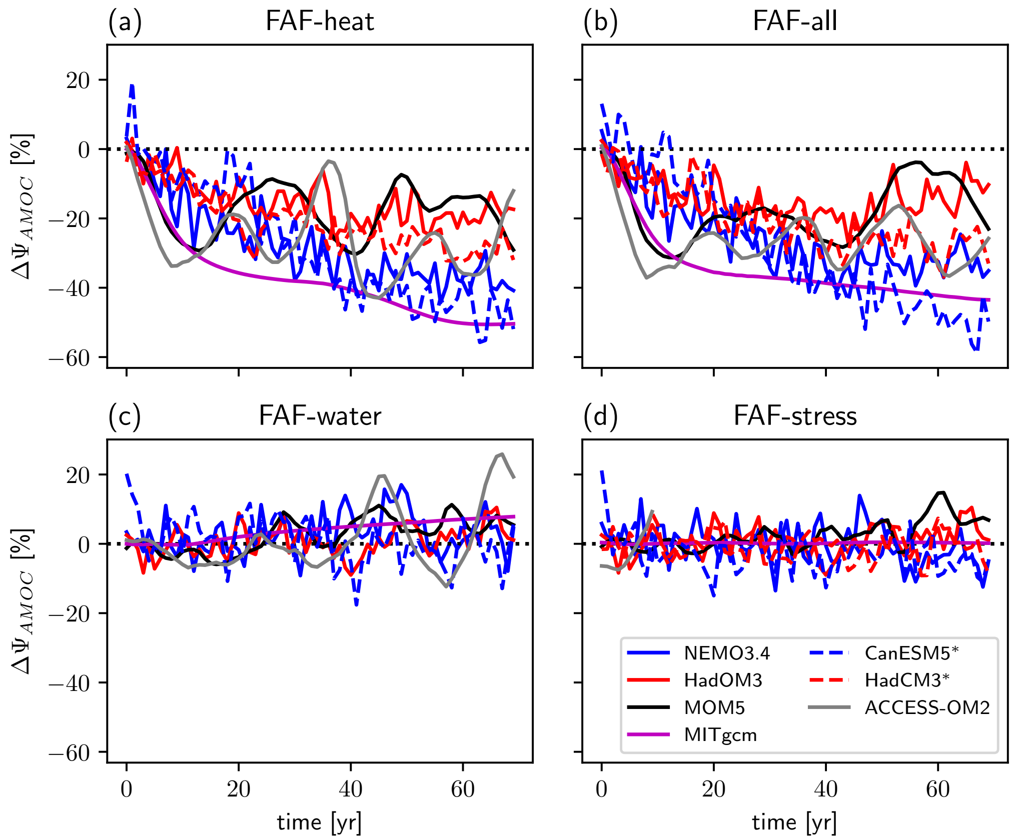

Figure 2. Atlantic meridional overturning circulation (AMOC) strength change, $\Delta\Psi_{AMOC}$ (Huber & Zanna, 2017), versus time for FAF-heat (a), FAF-all (b), FAF-water (c) and FAF-stress (d) relative to FAF-control. Blue (NEMO3.4/CanESM5) and red (HadOM3/HadCM3) lines indicate ocean-only (solid) and coupled, atmosphere-ocean (dashed) simulations, respectively. Solid and dashed magenta lines denote two MOM simulations, MOM5 and ACCESS-OM2, respectively. The dotted black line indicates $\Delta\Psi_{AMOC} = 0$, with individual models colours as in the legend.

heat typically slows over time, consistent with more realistic, coupled AOGCM simulations under greenhouse gas forcing (Collins et al., 2013). After 60 years in FAF-heat, $\Delta\Psi_{AMOC}$ ranges between -20% to -50%. This AMOC response spread suggests differences in model sensitivity to identical surface perturbations is relatively high, in contrast to (Huber & Zanna, 2017).

For the two pairs of coupled atmosphere-ocean and ocean only simulations, AMOC weakening is 10% larger in the coupled relative to the ocean-only configuration. The MITgcm, MOM5 and ACCESS-OM2 cases demonstrate substantially less $\Delta\Psi_{AMOC}$ interannual variability in comparison to other ensemble members. This is likely due to the relatively low frequency, monthly FAF-control background surface fluxes (Q, W and τ) which are linearly interpolated to daily frequency and applied in MITgcm, MOM5 and ACCESS-OM2. Weak SST and SSS restoring is also applied in MITgcm and ACCESS-OM2, which acts mitigate high frequency variability. In contrast, daily and sub-daily FAF-control surface fluxes from an interactive atmosphere are applied in HadOM3/HadCM3 and NEMO3.4/CanESM5, respectively.

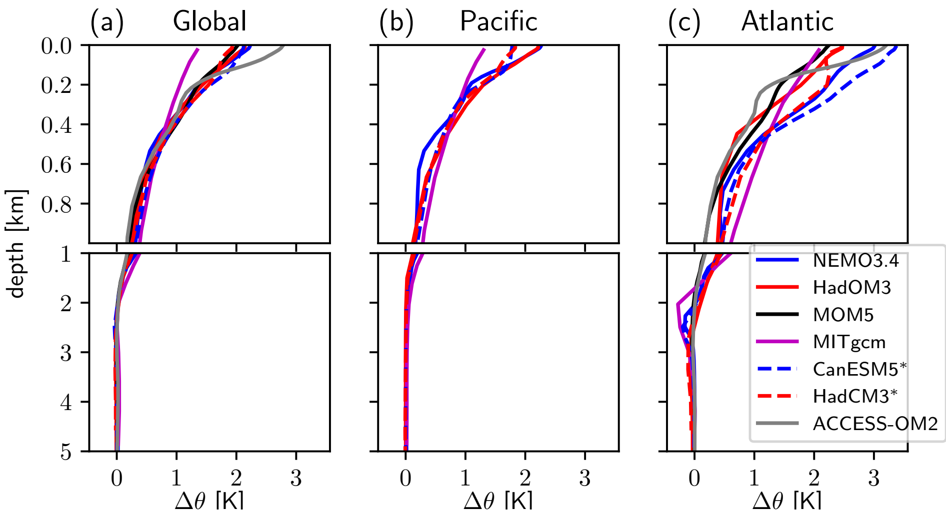

Figure 3. Vertical profiles of mean temperature change in FAF-heat year 61-70 minus FAF-control for the global (a), Pacific (b) and Atlantic (c) ocean. For each figure, the upper panel shows the upper 1 km, with the lower panel showing 1-5 km depth. Line colours and styles are defined in the legend, with dashed blue and red lines denoting the coupled, AOGCM simulation.

In each model, the barotropic streamfunction decreases along the western boundary of the North Atlantic in FAF-heat and increases near the subpolar gyre (not shown). This suggests a general weakening of the North Atlantic subtropical and subpolar gyre circulation, which is consistent with the simulated AMOC weakening (Figure 2(a)). There is no consensus amongst the ensemble of a change in the Antarctic circumpolar current (ACC) strength, measured by the Drake Passage transport, Ψ_{ACC} (Huber & Zanna, 2017). Some models indicate a very strong Ψ_{ACC} weakening, such as ACCESS-OM2 (-7.7%) and MOM5 (-12.4%), whilst the other models show only small changes (weakening or strengthening): NEMO3.4 (-0.7%), MITgcm (0.2%), HadOM3 (1.3%) CanESM5(1.6%) and HadCM3 (1.7%). Changes in the Antarctic bottom water (AABW) overturning, Ψ_{AABW} (defined as the minimum of the global meridional overturning streamfunction beneath 500 m and north of 40°S) range between -3.8% to 3.1%, indicating no multi-model consensus and relatively small changes in this suite of models.

3.2 Ocean Heat Content

In the FAF-heat simulation, global mean and basin scale warming after 60 years is largely confined to the upper 1000 m (Figure 3). The vertical profile of global mean temperature change beneath 400 m is generally consistent across the ensemble. Global mean SST warming is approximately 2°C in MOM5, HadOM3, NEMO3.4, HadCM3 and CanESM5. MITgcm and ACCESS-OM2 are outliers, with global mean SST warming of 1.1°C and 2.8°C, respectively. Pacific mean vertical profiles of temperature change are similar to the global profiles beneath 200 m. However, in the upper layers of Pacific, the two coupled simulations (CanESM5 and HadCM3) indicate less warming relative to the corresponding ocean-only (NEMO3.4 and HadOM3) simulations, with a mean difference in SST change of -0.5°C. An opposite response occurs in the Atlantic, with relatively more warming in the upper layers of the coupled versus ocean-only simulations. As in the global mean, MITgcm is an outlier compared to the rest of the ensemble, with less surface warming in the Atlantic but a deeper penetration of >0.5°C warming, potentially due to the vertical resolution of the models or vertical mixing parameterisations.

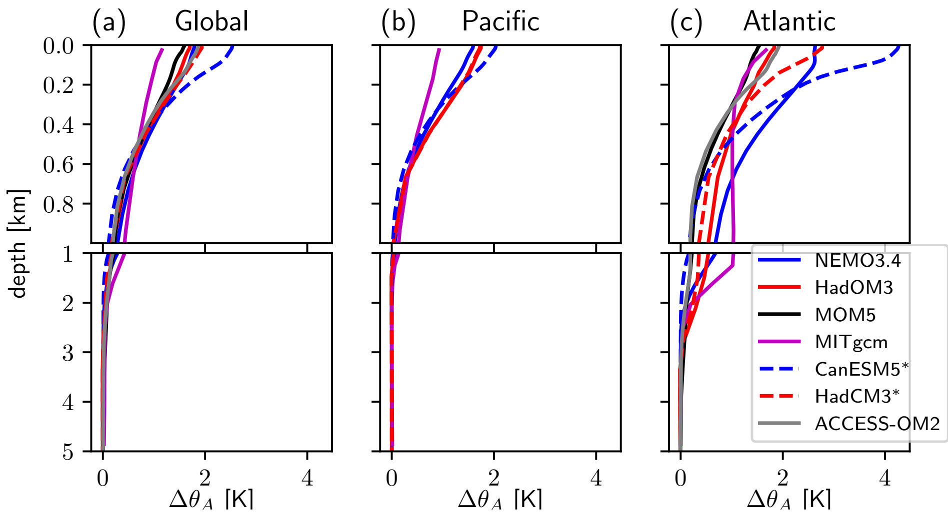

Figure 4. As in Figure 3, except for added temperature change in FAF-heat year 61-70 minus FAF-control.

Global and basin scale vertical profiles of FAF-heat temperature changes are typically consistent with corresponding vertical profiles of added temperature changes (Figure 4). In particular, warming from surface added temperature changes in the Atlantic is intensified in coupled models. This is linked to the enhanced AMOC weakening in AOGCMs, which leads to less downward advection of added temperature changes relative to OGCMs. Similarities between temperature and added temperature change suggests that heat content change at basin scales is largely due to the passive advection and diffusion of a net heat input at the surface, consistent with previous coupled FAFMIP simulations (Gregory et al., 2016). In contrast to basin scale total and added temperature changes, corresponding redistributed temperature changes are relatively small (not shown), with global mean absolute redistributed SST changes less than 0.5°C.

Ocean heat content change at each grid point is defined as $\Delta OHC = c_p \rho_0 \Delta\theta A \delta z$, assuming $c_p = 4000$ J K^{-1} kg^{-1} is a fixed specific heat capacity, $\rho_0 = 1035$ kg m^{-3} is a constant reference density, $\Delta\theta$ is the temperature change, A is the surface area and δz is layer thickness. Regional patterns of the depth integrated total, added and redistributed ocean heat content change in FAF-heat are shown in Figures 5-7, respectively. All models indicate increased total heat content in the mid-latitude relative to the high-latitude Southern Ocean where there is a net surface heat input. The pattern and magnitude of Southern Ocean total heat content change is similar to the added heat content change (Figure 6), whilst the redistributed heat content change has a much smaller magnitude in this region. This suggests that Southern Ocean heat content change is largely due to northward Ekman transport and subduction of heat input at high latitudes (Armour et al., 2016; Gregory et al., 2016; Zanna et al., 2019). The similarity between OGCM and AOGCM ΔOHC implies that the atmospheric feedback in coupled simulations has a minimal role in affecting heat content in the Southern Ocean.

The North Atlantic demonstrates the largest spread across the ensemble in the pattern of ocean heat content change. This is linked with the large spread in simulated AMOC changes (Figure 2(a)), which modulates the northward heat flux into the North Atlantic. A region of substantial heat loss in MITgcm, MOM5, ACCESS-OM2, and to a lesser extent in HadOM3, is present in the mid-latitude North Atlantic. In contrast, NEMO3.4 and the two coupled simulations indicate increased heat content in this region. Examining the added and redistributed heat content patterns in the North Atlantic, we see that the total heat content change is a small residual of the sum of these two terms. The

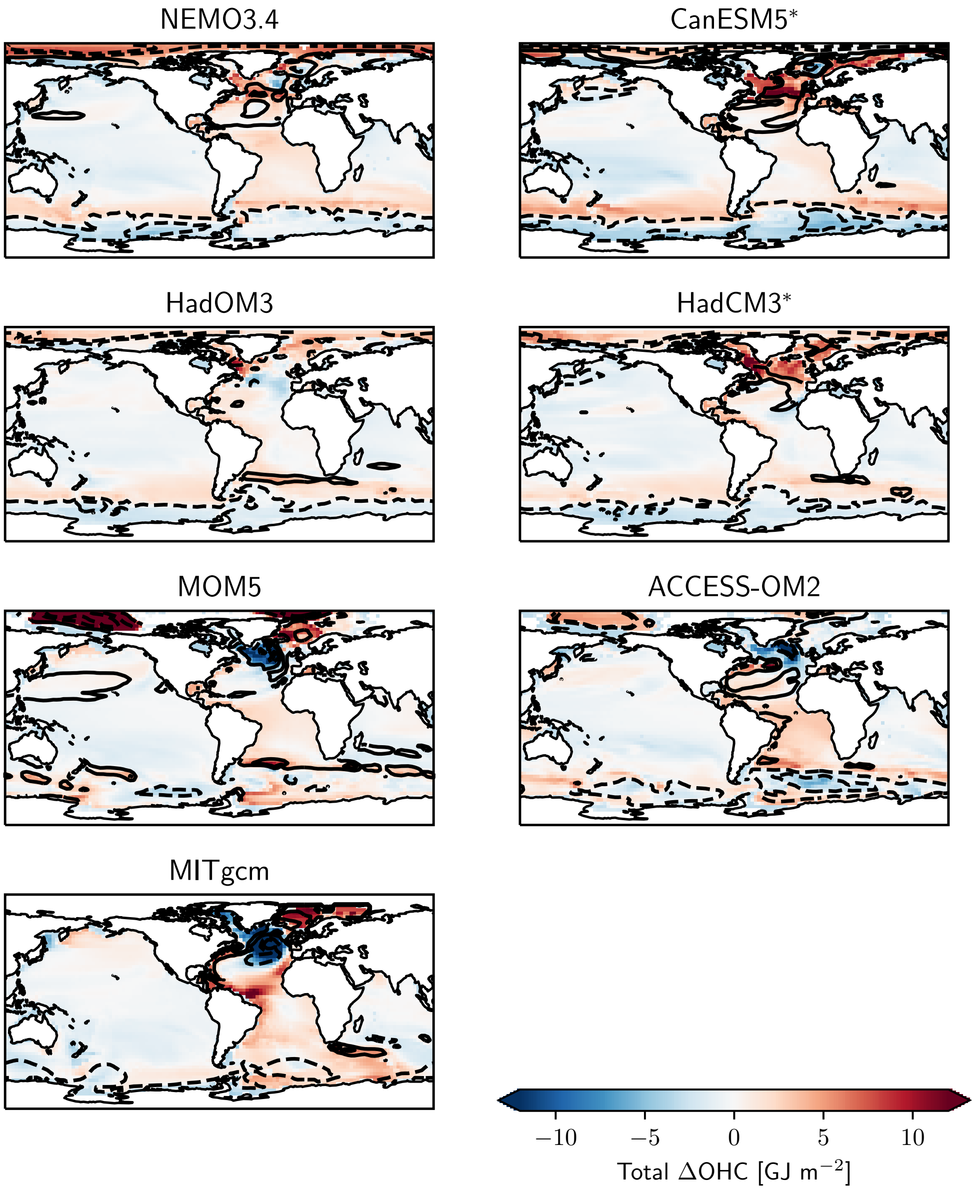

Figure 5. Colours show the depth integrated FAF-heat minus FAF-control year 61-70 mean ocean heat content change in GJ m^{-2} (1 GJ $\equiv$ 10^9 J), with the global mean (3.6 GJ m^{-2}) subtracted, for each model. Coupled models are indicated with a *. Black contours denote the corresponding FAF-heat minus FAF-control year 61-70 mean dynamic sea level change, $\Delta\zeta$, at 0.1 m intervals. Dashed and solid lines denote negative $\Delta\zeta$ and positive $\Delta\zeta$, respectively.

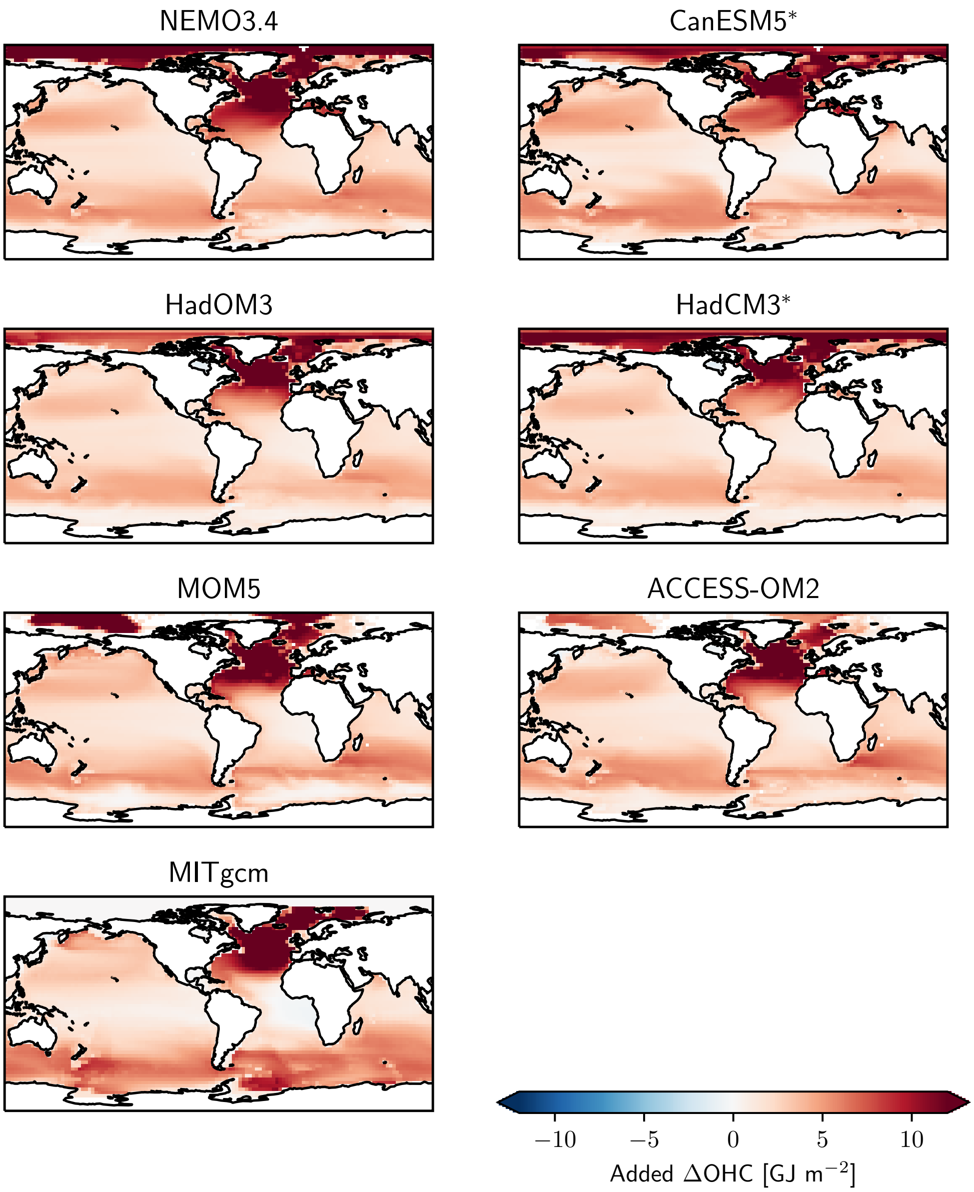

Figure 6. Depth integrated added heat content change [GJ m^{-2}] year 61-70 FAF-heat minus FAF-control.

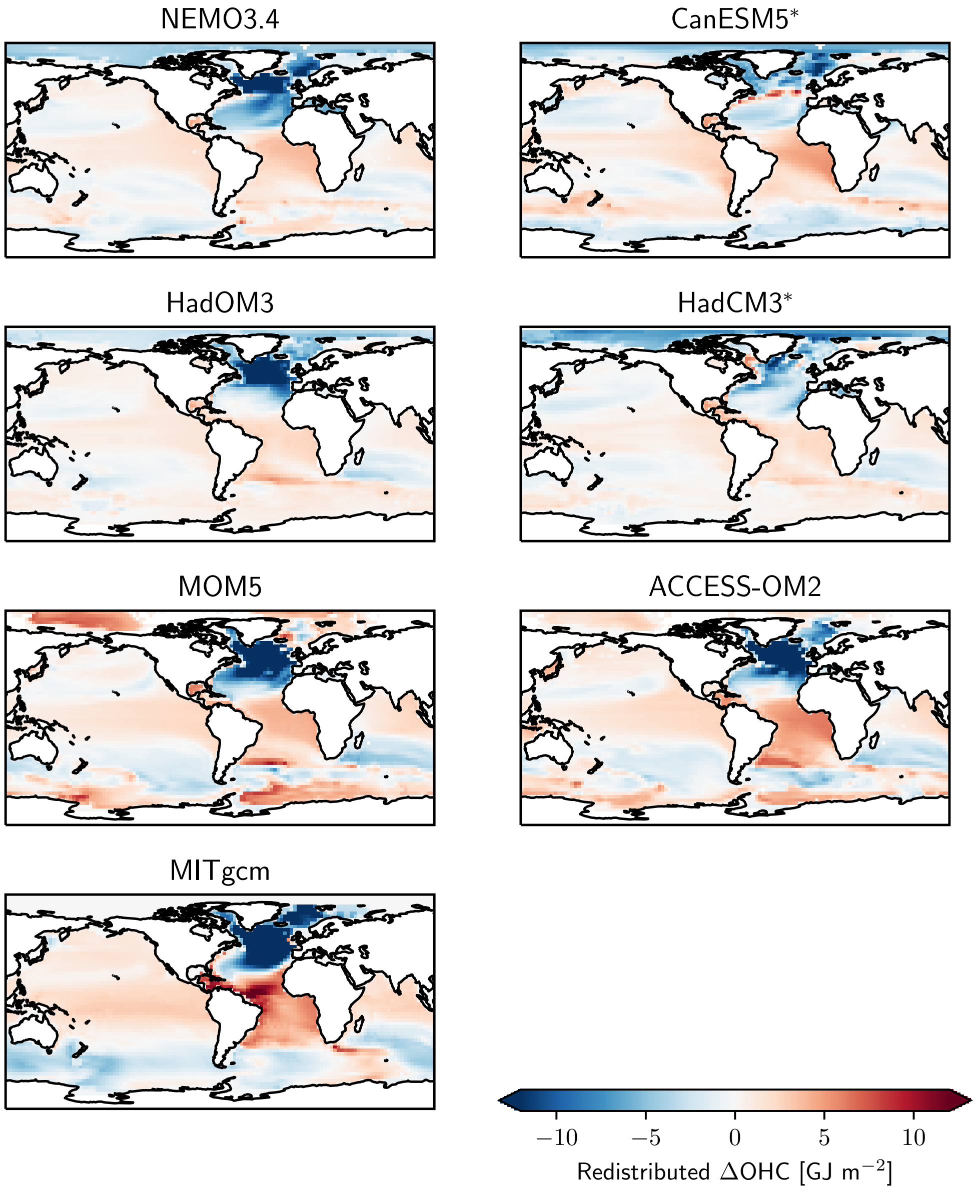

Figure 7. Depth integrated redistributed heat content change [GJ m^{-2}] year 61-70 FAF-heat minus FAF-control.

spread in added heat content, which warms the North Atlantic, is much smaller than the spread in redistributed heat content, which generally cools the mid-latitude North Atlantic, due to the reduced northward heat transport by the weakened AMOC. In the two MOM simulations, MOM5 and ACCESS-OM2, the main difference is the background state. The redistributed heat content change is of a larger magnitude across the Atlantic in ACCESS-OM2 relative to MOM5. These results suggest that differences in circulation change, and the background circulation, are primary in setting the heat content change in the North Atlantic.

Comparing the ocean-only and coupled cases, we find that there is a greater depth integrated total heat content increase in the mid-latitude North Atlantic, and less decreased heat content in the tropical Atlantic, in the latter. In the mid-latitude North Atlantic, added heat content increases (Figure 6) are slightly weaker in the coupled simulations, whilst redistributed heat loss (Figure 7) is much weaker. However, it is important to note that in AOGCMs the redistributed heat change also includes the effect of additional air-sea heat flux changes from the atmospheric feedback. Examining the vertical profile of redistributed temperature change, $\Delta\theta_R$, reveals that North Atlantic cooling is more concentrated and stronger near the surface in AOGCMs in comparison to OGCMs. Consequently, in AOGCMs, the surface θ_R minus air temperature gradient is steeper relative to the implicit SST minus air temperature gradient contributing to the atmosphere-ocean heat flux in OGCMs. This leads to an additional surface heat input at high latitudes from the atmosphere in coupled simulations, relative to ocean-only simulations. In the tropical Atlantic, θ_R warming is more concentrated near the surface in AOGCMs relative to OGCMs. Hence, in AOGCMs, there is additional heat loss to the atmosphere over the tropical Atlantic, which is balanced by the extra heat input at higher latitudes.

In the Pacific, the ocean heat content change is typically more homogeneous than in the Atlantic and Southern oceans across the multi-model ensemble, at approximately 1-2 GJ m^{-2}. Similar to the Atlantic, Pacific warming from added heat is typically larger at high latitudes (3-4 GJ m^{-2}) and weaker at low latitudes (0-1 GJ m^{-2}). This added heat content change pattern is offset by a slight cooling due to redistribution at high latitudes, and a warming from redistribution in the tropics.

The surface heat flux change in AOGCMs is tightly coupled to the AMOC change. Total heat gain and loss at high and low latitudes in the Atlantic, respectively, weakens the meridional density gradient, causing the AMOC to weaken. This AMOC weakening reduces northward heat transport, which leads to further surface θ_R cooling at high latitudes and warming at low latitudes, contributing to the AMOC weakening in coupled models. This mechanism is consistent with the simulated 10% additional AMOC weakening in AOGCMs relative to the OGCMs (Figure 2(a)). Consequently, the atmospheric feedback due to heat redistribution acts to enhance AMOC weakening in AOGCMs by slightly amplifying the prescribed surface heat flux perturbation.

The time and depth weighted 70 year mean FAF-heat minus FAF-control temperature tendency terms are now examined to assess which processes contribute to the ΔOHC patterns. Figure 8 demonstrates the ensemble mean and standard deviation of the total temperature tendency change, $\Delta\partial_t\theta$, whose time-integral is identical to ΔOHC in heat flux units by definition. The FAFMIP temperature tendency diagnostics enable the decomposition:

$$\Delta\partial_t\theta = \Delta\partial_t\theta_{resolved} + \Delta\partial_t\theta_{eddy} + \Delta\partial_t\theta_{isopycnal} + \Delta\partial_t\theta_{diapycnal} + \Delta\partial_t\theta_{surface}. \quad (4)$$

Here, $\Delta\partial_t\theta_{resolved}$, $\Delta\partial_t\theta_{eddy}$, $\Delta\partial_t\theta_{isopycnal}$ and $\Delta\partial_t\theta_{diapycnal}$ are the temperature tendency changes due to resolved advection, parametrised eddy advection, isopycnal diffusion and diapycnal diffusion changes, respectively. Temperature tendency changes in the surface layer due to the atmosphere-ocean heat flux perturbation are represented by

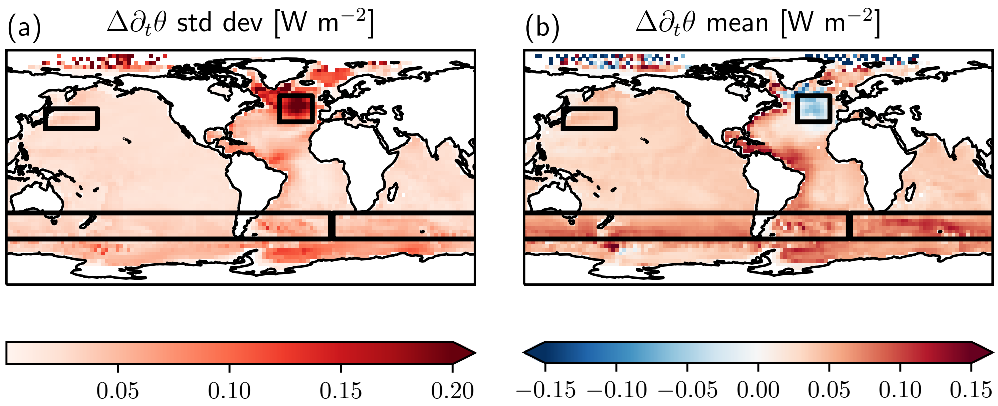

Figure 8. Depth-weighted and year 1-70 mean FAF-heat minus FAF-control total temperature tendency change for the multi-model ensemble standard deviation (a) and mean (b). Black boxes indicate the North Atlantic, North Pacific and Southern Ocean regions.

$\Delta\partial_t\theta_{surface}$. Three case study regions are selected for further analysis: the mid-latitude North Atlantic, which shows the largest spread in $\Delta\partial_t\theta$ and a multi-modl mean heat loss, the western North Pacific over the subtropical gyre, with moderate heat increase and ensemble spread, and the low-latitude Southern Ocean between 35°S to 55°S, as shown in Figure 8. For each of these case study regions, $Q' > 0$ and hence $\Delta\partial_t\theta_{surface} > 0$. Beneath the surface layer, $\Delta\partial_t\theta_{surface} = 0$ by definition, and as the surface layer thickness varies across the ensemble (6-50 m), the depth weighted mean of $\Delta\partial_t\theta_{surface}$ also varies (Figure 9).

For the mid-latitude North Atlantic region (Figure 9), MITgcm and MOM5 simulate $\Delta\partial_t\theta < 0$, whereas HadOM3, HadCM3, NEMO3.4 and CanESM5 all simulate $\Delta\partial_t\theta > 0$. In every model, the $\Delta\partial_t\theta_{resolved}$ contribution to $\Delta\partial_t$ is negative. This cooling due to resolved advection is consistent with the simulated AMOC weakening under FAF-heat (Figure 2), which reduces northward heat transport in the North Atlantic. The cooling is approximately one quarter opposed by a positive contribution to $\Delta\partial_t$ due to parametrised eddy advection from the GM scheme. Exarchou et al. (2015) found a similar large negative contribution to the North Atlantic heat budget due to weakened residual mean advection. Generally, the sign of $\Delta\partial_t\theta_{diapycnal}$ is consistent with $\Delta\partial_t$. However, there is broad spread in all temperature tendency terms across the ensemble, suggesting that no single process dominates heat content change in the mid-latitude North Atlantic, consistent with the findings of Exarchou et al. (2015) who analysed three different AOGCMs.

In the western North Pacific subtropical gyre region (Figure 8), all models simulate $\Delta\partial_t\theta > 0$, however, there is large spread in the magnitude of the heat content change across the ensemble. There is no consistency between $\Delta\partial_t\theta > 0$ and the sign of any single component in the heat budget decomposition (Equation 4). For example, the large heat increase in HadCM3, $\Delta\partial_t\theta = 0.07$ W m^{-2}, is mainly driven by resolved advection change, $\Delta\partial_t\theta_{resolved} = 0.065$ W m^{-2} . In contrast, heat increase in HadOM3, $\Delta\partial_t\theta = 0.035$ W m^{-2}, is mainly a balance of diapycnal diffusion, 0.05 W m^{-2}, and resolved advection, -0.02 W m^{-2}, changes. This highlights a substantial contrast in the heat content change processes between a matching AOGCM/OGCM pair of models. Generally, across the ensemble, spread in the individual processes contributing to heat increases in the western North Pacific typically cancels, resulting in only small spread for $\Delta\partial_t\theta$.

For the low-latitude Southern Ocean, where increased heat content is simulated in all cases, a more consistent result is evident in contrast to the mid-latitude North Atlantic and western North Pacific. In all models, heating from $\Delta\partial_t\theta_{isopycnal}$, and to a lesser

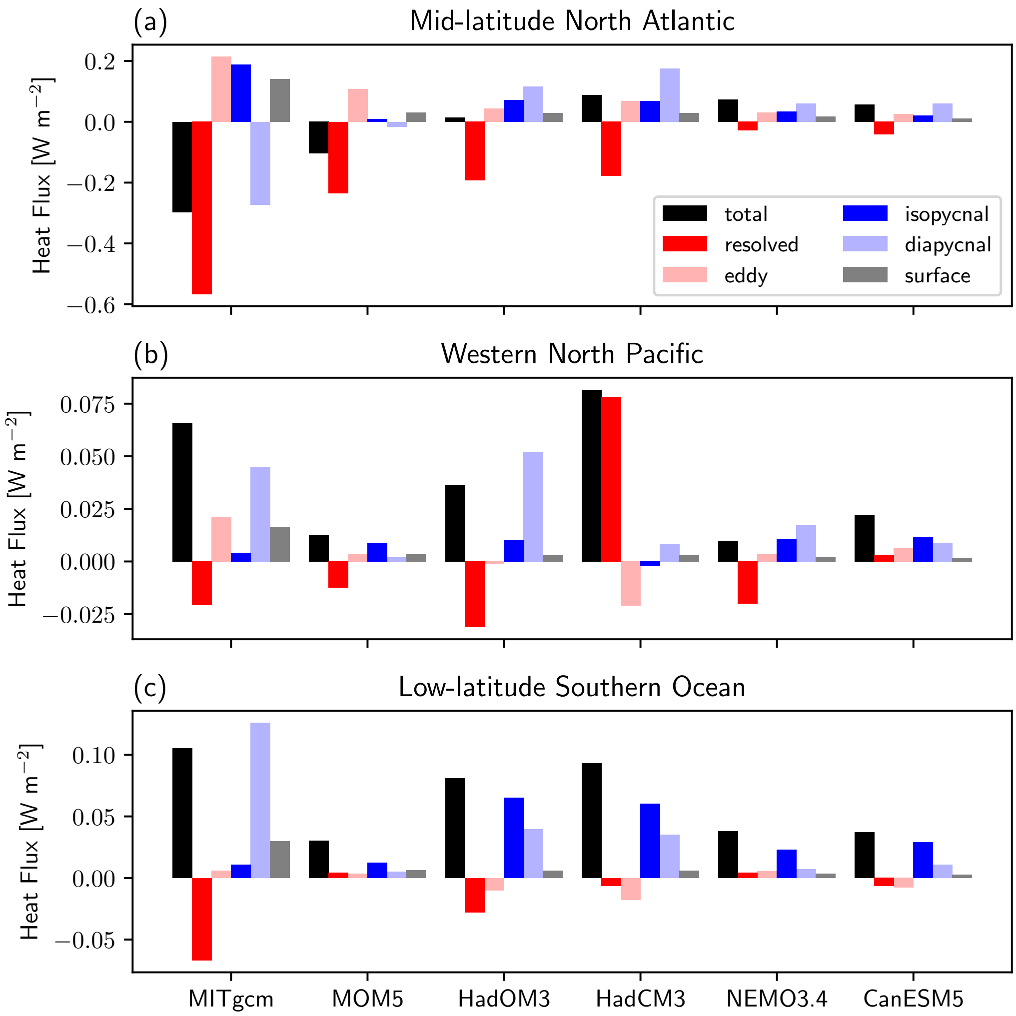

Figure 9. Area and depth-weighted mean components (Equation 4) of the FAF-heat minus FAF-control temperature tendency change for the North Atlantic (a), North Pacific (b) and Southern Ocean (c) regions, as presented in Figure 8.

extent $\Delta\partial_t\theta_{diapycnal}$, largely determine the magnitude of $\Delta\partial_t\theta$. MITgcm is an outlier, where heating from diapycnal diffusion change exceeds isopycnal diffusion change. Notably, both the resolved and parametrised eddy advection terms are much smaller than $\Delta\partial_t\theta$, or weakly negative in all cases. This suggests that residual mean advection changes in FAF-heat play a minimal role in setting the low-latitude Southern Ocean warming. This contrasts the findings of Kuhlbrodt et al. (2015), who showed that subtropical Southern Ocean warming is mainly due to residual mean advection changes, whilst higher-latitude Southern Ocean warming is largely due to reduced vertical isopycnal diffusion. However, this study examines a broader latitude band than Kuhlbrodt et al. (2015) and focuses on total isopycnal diffusion changes instead of just the vertical component, perhaps explaining the disparity. Furthermore, the dominance of total isopycnal diffusion change in the Southern Ocean heat budget in FAF-heat is broadly consistent with the findings of Gregory (2000) and Exarchou et al. (2015).

3.3 Dynamic Sea Level

Across the ensemble, the FAF-heat simulated DSL change, $\Delta\zeta$, is generally a 20 cm fall across the high latitude Southern Ocean and a weaker, 10 cm rise across much of the tropical and subtropical Atlantic, as shown by the contour lines in Figure 5. Over the North Pacific, a relative sea level rise of 10 cm is consistently simulated over the subtropical gyre, with a relative sea level fall of approximately 8 cm simulated over the subpolar gyre. Similar to ocean heat content change, the largest $\Delta\zeta$ spread is over the North Atlantic, consistent with the findings of Gregory et al. (2016). In MITgcm, MOM5 and ACCESS-OM2, a relative sea level fall is simulated over the North Atlantic subpolar gyre, with a relative sea level rise over the subtropical gyre. In contrast, HadOM3 and HadCM3 simulate a sea level rise over the subpolar gyre, and a weaker relative sea level fall at mid-latitudes. NEMO3.4 and CanESM5 both simulate a relative sea level rise across much of the North Atlantic.

Bouttes et al. (2013) suggest the simulated DSL change pattern of relative sea level rise over the subpolar gyre and fall over the subtropical gyre under CO_2 forcing is largely due to the surface heat flux change. Simulated temperature and salinity changes in FAF-heat are used to decompose DSL changes into steric, $\Delta\theta_{steric}$, thermosteric, $\Delta\zeta_\theta$, and halosteric, $\Delta\zeta_S$, contributions (Pardaens et al., 2011) using a nonlinear equation of state (TEOS-10, McDougall and Barker (2011)). Simulated DSL changes are almost entirely steric, with a negligible contribution from barotropic changes (not shown). The halosteric DSL change (Figure 11) largely balances the thermosteric (Figure 10) DSL change, leaving the steric DSL change as a small residual (Lowe & Gregory, 2006). The thermosteric DSL change closely resembles the total heat content change (Figure 5). Both the thermosteric and halosteric components show substantial spread in the North Atlantic, each contributing to the large spread in simulated DSL change.

4 FAF-water, FAF-stress and FAF-all Intercomparison

This section explores the ocean's response in the FAF-water, FAF-stress and FAF-all experiments. Similar to Section 3, analysis focuses on the mean simulated change during years 61-70.

4.1 Ocean Circulation

Simulated AMOC weakening across the ensemble is of a similar order of magnitude in FAF-all, 20-50%, as in FAF-heat, as shown by Figure 2(b). This suggests that the addition of surface freshwater and momentum fluxes in OGCMs has only a secondary effect to surface heat fluxes in modulating AMOC changes (as found for AOGCMs (Gregory et al., 2016)). After 60 years in FAF-water and FAF-stress, $\Delta\Psi_{AMOC}$ typically has a magnitude smaller than 10% of $\Delta\Psi$. Examining ACC changes, in FAF-stress there is a consistent strengthening (between 3% to 7%), with FAF-water demonstrating a weakening

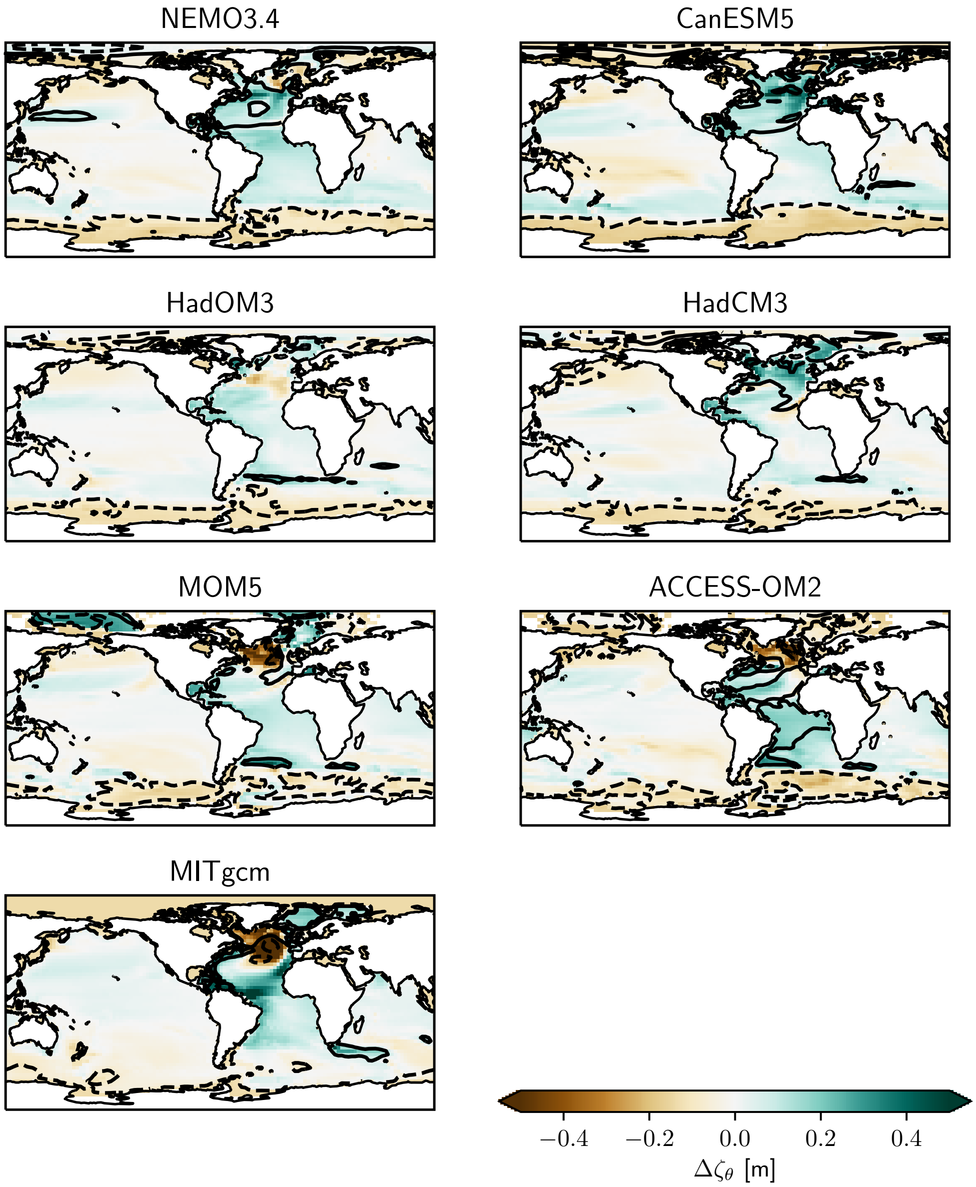

Figure 10. Colours show the FAF-heat minus FAF-control year 61-70 mean thermosteric component, $\Delta\zeta_\theta$, of the dynamic sea level change. Black contours denote the corresponding steric component, $\Delta\zeta_{steric}$, of the dynamic sea level change, at 0.1 m intervals. Dashed and solid lines denote negative $\Delta\zeta_{steric}$ and positive $\Delta\zeta_{steric}$, respectively.

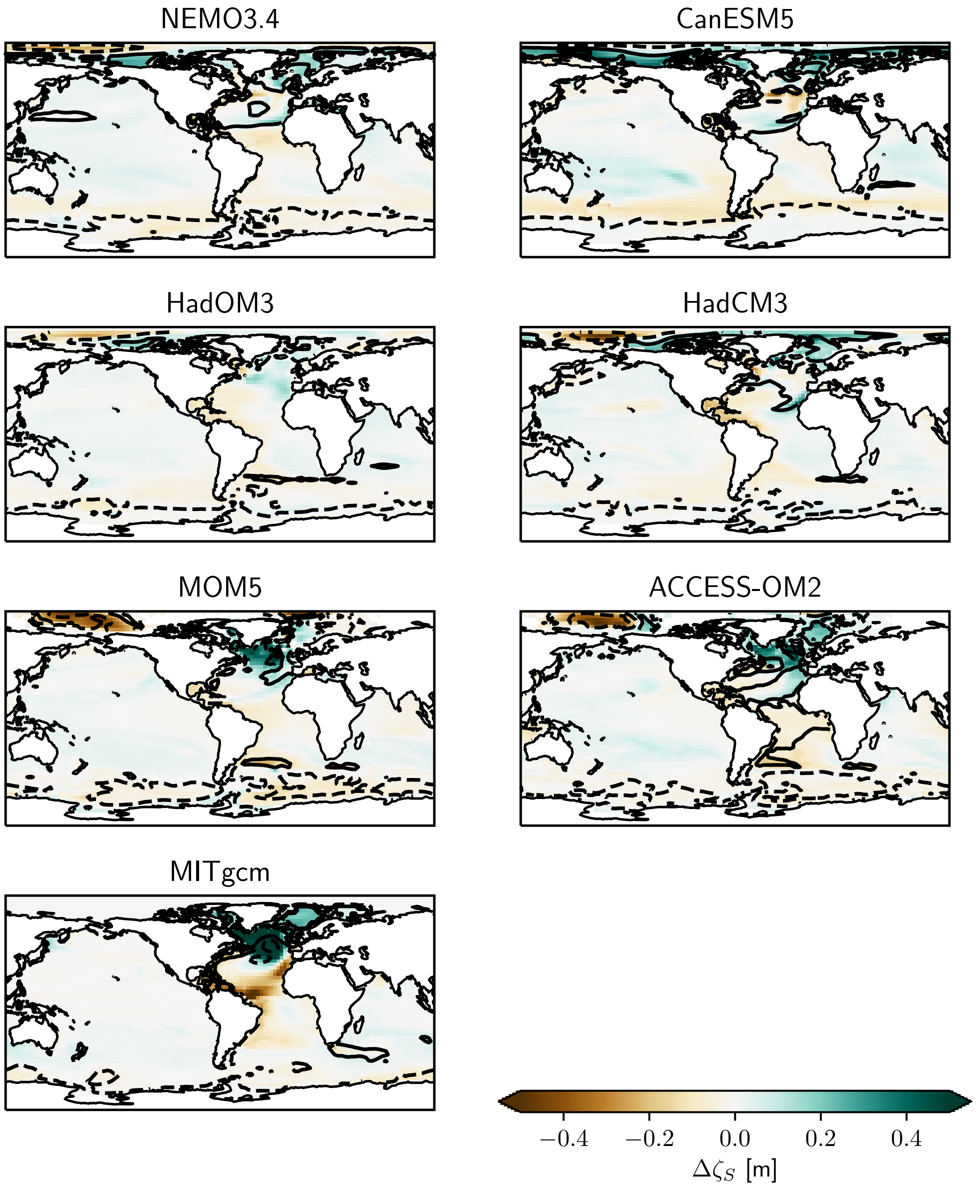

Figure 11. Colours show the FAF-heat minus FAF-control year 61-70 mean halosteric component, $\Delta\zeta_\theta$, of the dynamic sea level change. As in Figure 10, black contours indicate $\Delta\zeta_{steric}$.

(-2% to -13%). The ACC change in FAF-all demonstrates no consistency amongst the ensemble, with only relatively weak magnitudes (-3% to 2%). However, the individual surface flux perturbations combine relatively linearly, with wind-driven strengthening of the ACC largely cancelled by the freshwater flux-driven weakening (not shown). All models simulate a weakening of AABW overturning in FAF-water (-0.8% to -18%), and a strengthening of AABW overturning in FAF-stress (3% to 20%) . Examining the FAF-all AABW overturning response, there is no consistency amongst the ensemble (-18% to 21%), however the FAF-heat, FAF-water and FAF-stress responses combine relatively linearly (not shown). This results suggest that ACC and AABW overturning changes are linked, which is consistent with geostrophic balance.

4.2 Ocean Heat Content and Dynamic Sea Level

FAF-water and FAF-stress ocean heat content changes, alongside corresponding dynamic sea level changes, are presented in Figures 12 and 13, respectively. An area of consensus in FAF-water is the Southern Ocean, where all models simulate heat loss at low latitudes and heat gain around the Antarctic coastline. This is complemented by a rise and fall in dynamic sea level at high and mid Southern Ocean latitudes, respectively, suggesting the DSL change in this region is largely thermosteric. Gregory et al. (2016) suggest the input of freshwater at high Southern Ocean latitudes in FAF-water acts to stratify the water column, reducing upward convection and surface heat loss.

A second area of consensus in FAF-water is the western subtropical North Atlantic, where all models simulate moderate heat increases, of approximately one quarter the corresponding heat increases simulated in FAF-heat. In all models except for NEMO3.4, this region of warming is collocated with a fall in dynamic sea level. This implies that the negative halosteric component, from increased salinity, typically has a larger magnitude than the positive thermosteric component, from increased temperature. In CanESM5, HadCM3 and MITgcm, the pattern of heat content increases in the North Atlantic extends northwards into the mid-latitude and subpolar regions. In contrast, the other four ensemble members simulate a weak heat loss in the mid-latitude and subpolar North Atlantic. Since no surface heat perturbation is included in FAF-water, the heat content change is entirely due to circulation change leading to heat redistribution.

Similar to FAF-water, patterns of ocean heat content change are relatively weak in FAF-stress, in comparison to FAF-heat. As in FAF-water, the Southern Ocean is a major area of consensus in FAF-stress, but with the opposite pattern: heat loss and DSL fall, and heat increases and DSL rise, at high and mid-latitudes, respectively. This pattern in the Southern Ocean can be explained by the enhanced northward Ekman transport in FAF-stress, due to the increased surface westerly wind stress, causing a passive advection of heat from the high to mid-latitudes. Consequently, in the ocean-only ensemble, the FAFMIP momentum flux perturbation acts to increase the DSL gradient in the Southern Ocean, whilst the freshwater perturbation weakly weakens the DSL gradient, consistent with previous studies (Bouttes & Gregory, 2014; Saenko et al., 2015). An area of major disagreement in FAF-stress is the North Atlantic, where there is no consensus on the pattern of ocean heat content or $\Delta\zeta$ change. However, the magnitude of the spread in FAF-stress North Atlantic responses is much smaller than in both FAF-heat and FAF-water. This suggests that the uncertain response to surface momentum flux perturbations is of second order to the uncertainty in the overall heat content change and $\Delta\zeta$ response.

There is strong similarity between the FAF-heat (Figure 5) and FAF-all (Figure 14) patterns of ocean heat content and $\Delta\zeta$. This is consistent with previous studies, suggesting uncertainty in patterns of ocean heat content change and corresponding $\Delta\zeta$ change is largely driven by uncertainty in the response to surface heat flux perturbations (Lowe & Gregory, 2006; Gregory et al., 2016), as discussed in Section 3. Furthermore, there is AMOC response similarity between FAF-heat and FAF-all.

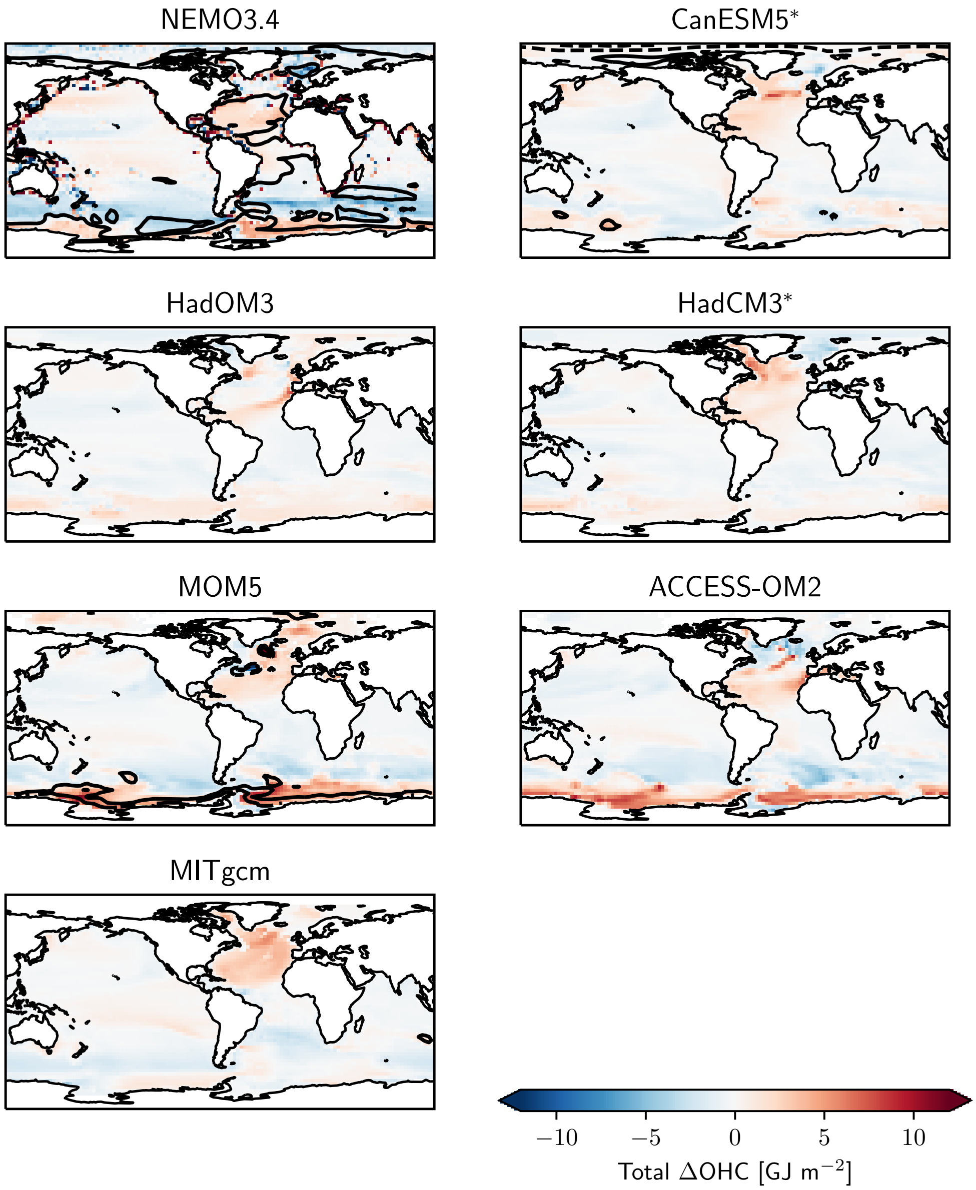

Figure 12. Colours show the depth integrated FAF-water minus FAF-control year 61-70 mean ocean heat content change in GJ m^{-2} for each model, with coupled models indicated by a *. Contour lines as in Figure 5, except showing $\Delta\zeta$ at 0.05 m intervals.

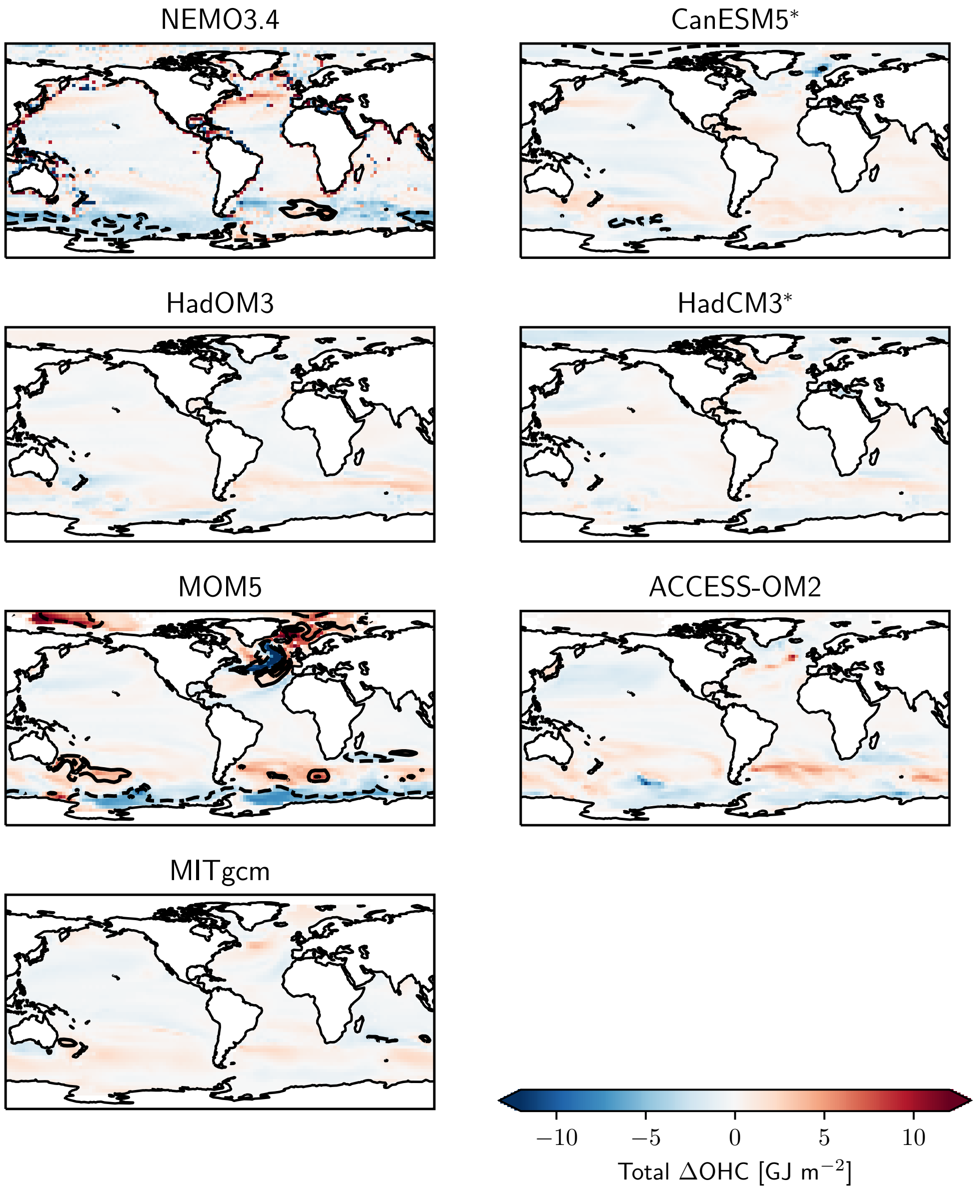

Figure 13. Colours show the depth integrated FAF-stress minus FAF-control year 61-70 mean ocean heat content change in GJ m^{-2} for each model, with coupled models indicated by a *. Contour lines as in Figure 5, except showing $\Delta\zeta$ at 0.05 m intervals.

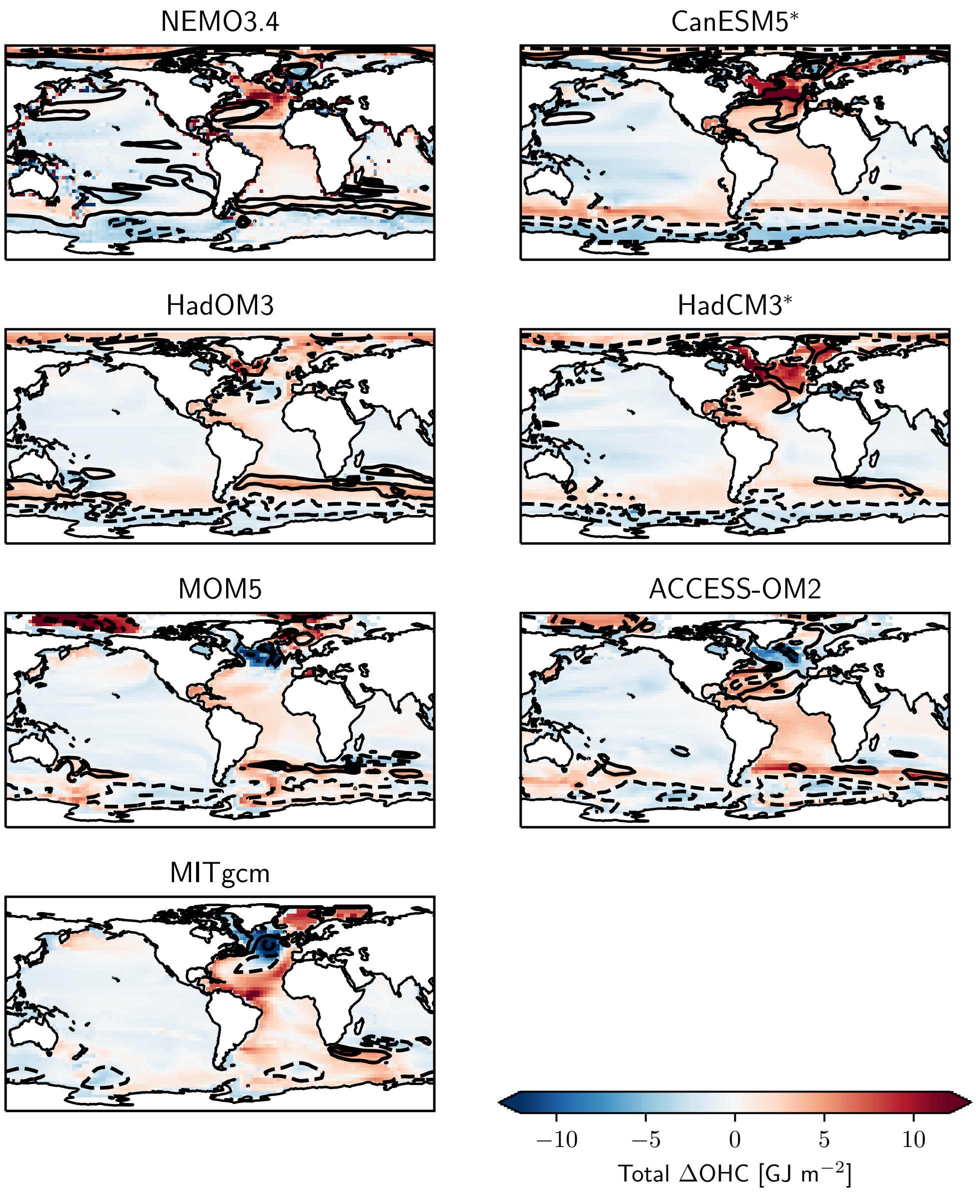

Figure 14. Colours show the depth integrated FAF-all minus FAF-control year 61-70 mean ocean heat content change in GJ m^{-2} for each model, with coupled models indicated by a *. Contour lines as in Figure 5, except showing $\Delta\zeta$ at 0.1 m intervals.

5 Conclusions

This study has examined the ocean response to abrupt surface momentum and buoyancy flux perturbations in an ensemble of OGCMs and AOGCMs. Consistent with previous studies, circulation change in the North Atlantic is mainly due to surface heat flux changes, with a minimal wind-driven response (Bouttes et al., 2013). In the FAF-heat simulation, where a model-independent surface heat flux perturbation is applied, there is a large spread (20-50%) in the simulated AMOC weakening amongst OGCMs. This builds upon the findings of Huber and Zanna (2017), who demonstrated that differences in surface heat flux changes dominate the spread in AMOC change. This study highlights a spread in the sensitivity of AMOC change to surface heat flux changes amongst different models. An important finding is that the coupled FAFMIP method (Bouttes & Gregory, 2014; Gregory et al., 2016) causes 10% additional AMOC weakening relative to the the ocean-only method. This enhanced AMOC weakening is due to an atmosphere-surface temperature redistribution feedback. As a result, the simulated surface heat flux change in coupled FAFMIP simulations is different from the FAF-heat perturbation over ocean regions where the circulation is particularly sensitive to surface heat flux changes (Delworth & Greatbatch, 2000).

This study indicates that the pattern of ocean heat content change is largely driven by surface heat flux changes, since the FAF-heat and FAF-all response is generally consistent. Amongst the OGCM ensemble, heat content change patterns are typically similar over the Southern Ocean and North Pacific. The North Atlantic is the region which demonstrates the largest spread in total ocean heat content change, itself a small residual of the added heat increase and redistributed heat loss. Added heat increase is largely passive, and hence is focussed in regions where the surface heat flux perturbation is positive, such as the North Atlantic and high latitude Southern Ocean. Generally, it is the spread in the redistributed heat content change, and hence circulation change, which dominates the spread in total heat content change. In the depth integral, AOGCMs simulate less redistributed cooling of the North Atlantic relative to OGCMs, despite greater AMOC weakening. However, redistributed changes are more concentrated near the surface in AOGCMs, contributing to a positive feedback to amplify the AMOC weakening.

Examining the temperature tendency diagnostics (Gregory et al., 2016), we find that warming in the low-latitude Southern Ocean across the ensemble is largely due to enhanced isopycnal and diapycnal diffusion, instead of residual mean advection change as suggested by previous studies (Lowe & Gregory, 2006; Bouttes & Gregory, 2014; Saenko et al., 2015; Marshall et al., 2015). However, this result is based on a depth weighted mean across a latitude band encompassing much of the residual overturning circulation. Hence, relatively coarse OGCMs may simulate the heat content change processes via isopycnal diffusion parametrisations instead of accurately resolving the overturning circulation. In the North Pacific, there is little agreement amongst the individual tendency terms, despite overall agreement of warming. Notably, HadCM3 and HadOM3 show a large difference due to the atmospheric feedback. In the former, substantial warming is almost entirely driven by residual mean circulation change. In contrast, the latter indicates warming is mainly as a balance of warming from diapycnal diffusion and cooling from resolved advection. Temperature tendencies for the North Atlantic highlight the important role that the spread in residual mean advection plays in setting the spread in heat content. Models with more AMOC weakening (MITgcm and MOM5) typically have a net cooling of the North Atlantic, whereas models with less AMOC weakening (NEMO3.4 and CanESM5) simulate a net warming. In all cases, the sign of the diapycnal diffusion change contribution is consistent with the sign of the total temperature tendency change.

Dynamic sea level changes in FAF-all, as with the ocean heat content changes, are mainly driven by the surface heat flux perturbation. Agreement amongst the OGCM ensemble over the Pacific sector of the Southern Ocean is relatively high, with between -3 to -4 GJ m^{-2} heat content change, contributing to $\Delta\zeta \approx -0.1$ m in each model via a negative thermosteric component. Over the North Atlantic, there is a wide spread in the DSL response, which is matched by large spread in both the thermosteric and halosteric components of $\Delta\zeta$. These salinity and temperature driven changes in DSL largely cancel (Lowe & Gregory, 2006; Pardaens et al., 2011), but both terms contribute to the overall spread. Comparing AOGCM and OGCM simulated dynamic sea level changes, the main inconsistencies over the North Atlantic are due to differences in the thermosteric response, which is related to the differences in heat content change and the atmospheric redistributed feedback amplifying the surface heat flux perturbation.

This study has shown that most of the spread in dynamic sea level and ocean heat content change arises due to different OGCM responses to surface heat flux perturbations. For the North Atlantic, this is strongly related to the sensitivity of the AMOC to buoyancy forcing. This highlights an important area of future investigation to improve our understanding of how North Atlantic surface heat fluxes and the AMOC respond to greenhouse gas forcing as a coupled system. An important finding is that using method B of Gregory et al. (2016) tends to amplify the prescribed surface heat flux perturbation. This leads to a stronger AMOC weakening in coupled models relative to ocean-only models due to atmosphere-ocean feedbacks. This result was speculated by Gregory et al. (2016), but this study has now quantified the enhanced AMOC weakening due to atmosphere-ocean feedbacks at 10%. Except for this relatively local feature in the North Atlantic, the ocean heat uptake and DSL response to buoyancy and momentum forcing is typically consistent for matching AOGCMs and OGCMs. This demonstrates that atmosphere-ocean feedbacks in coupled FAFMIP simulations typically have only a small effect on ocean heat content at basin scales, although they do strongly affect the North Atlantic.

Acknowledgments

AT, LZ, MC and JG are supported the Natural Environment Research Council (NERC) grant NE/R000727/1 (UKFAFMIP). LZ is also supported by the NERC grant NE/P019218/1. QW and JG are supported by the NERC grant NE/P019099/1 (TICTOC). KL and XZ are supported by the Centre for Southern Hemisphere Oceans Research (CSHOR), a joint research centre between the QNLM and the CSIRO. JC is supported by the CSHOR, and Australian Research Council's Discovery Project funding scheme (project DP190101173). All data used in this study, except for CanESM5 model output, is stored on the Centre for Environmental Data Analysis (CEDA) archive and is publicly available at: `http://gws-access.ceda.ac.uk/public/ukfafmip/`. CanESM5 model output produced for FAFMIP is available separately and publicly as part of the CMIP6 archive on the World Climate Research Programme's Earth System Grid Federation.

References

Armour, K. C., Marshall, J., Scott, J. R., Donohoe, A., & Newsom, E. R. (2016). Southern ocean warming delayed by circumpolar upwelling and equatorward transport. *Nature Geoscience*, *9*(7), 549-554. doi: 10.1038/ngeo2731

Bouttes, N., & Gregory, J. M. (2014). Attribution of the spatial pattern of CO2-forced sea level change to ocean surface flux changes. *Environmental Research Letters*, *9*(3), 034004. doi: 10.1088/1748-9326/9/3/034004

Bouttes, N., Gregory, J. M., Kuhlbrodt, T., & Smith, R. S. (2013). The drivers of projected north atlantic sea level change. *Climate Dynamics*, *43*(5-6), 1531-1544. doi: 10.1007/s00382-013-1973-8

Bouttes, N., Gregory, J. M., Kuhlbrodt, T., & Suzuki, T. (2012). The effect of windstress change on future sea level change in the Southern Ocean. *Geophysical Research Letters*, *39*(23). doi: 10.1029/2012gl054207

Church, J., Clark, P., Cazenave, A., Gregory, J., Jevrejeva, S., Levermann, A., ... Unnikrishnan, A. (2013). Sea Level Change. In T. F. Stocker et al. (Eds.), *Climate Change 2013: The Physical Science Basis. Contribution of Working Group I to the Fifth Assessment Report of the Intergovernmental Panel on Climate Change.* Cambridge University Press.

Chylek, P., Li, J., Dubey, M. K., Wang, M., & Lesins, G. (2011). Observed and model simulated 20th century arctic temperature variability: Canadian earth system model CanESM2. *Atmospheric Chemistry and Physics Discussions*, *11*(8), 22893-22907. doi: 10.5194/acpd-11-22893-2011

Collins, M., Knutti, R., Arblaster, J., Dufresne, J.-L., Fichefet, T., Friedlingstein, P., ... Wehner, M. (2013). Long-term Climate Change: Projections, Commitments and Irreversibility. In T. F. Stocker et al. (Eds.), *Climate Change 2013: The Physical Science Basis. Contribution of Working Group I to the Fifth Assessment Report of the Intergovernmental Panel on Climate Change.* Cambridge University Press.

Delworth, T. L., & Greatbatch, R. J. (2000). Multidecadal thermohaline circulation variability driven by atmospheric surface flux forcing. *Journal of Climate*, *13*(9), 1481-1495. doi: 10.1175/1520-0442(2000)013⟨1481:mtcvdb⟩2.0.co;2

Exarchou, E., Kuhlbrodt, T., Gregory, J. M., & Smith, R. S. (2015). Ocean heat uptake processes: A model intercomparison. *Journal of Climate*, *28*(2), 887-908. doi: 10.1175/jcli-d-14-00235.1

Flato, G., Marotzke, J., Abiodun, B., Braconnot, P., Chou, S., Collins, W., ... Rummukainen, M. (2013). Evaluation of Climate Models. In T. F. Stocker et al. (Eds.), *Climate Change 2013: The Physical Science Basis. Contribution of Working Group I to the Fifth Assessment Report of the Intergovernmental Panel on Climate Change.* Cambridge University Press.

Fox-Kemper, B., Danabasoglu, G., Ferrari, R., Griffies, S., Hallberg, R., Holland, M., ... Samuels, B. (2011). Parameterization of mixed layer eddies. III: Implementation and impact in global ocean climate simulations. *Ocean Modelling*, *39*(1-2), 61-78. doi: 10.1016/j.ocemod.2010.09.002

Fox-Kemper, B., Ferrari, R., & Hallberg, R. (2008). Parameterization of Mixed Layer Eddies. Part I: Theory and Diagnosis. *Journal of Physical Oceanography*, *38*(6), 1145-1165. doi: 10.1175/2007jpo3792.1

Gaspar, P., Grégoris, Y., & Lefevre, J.-M. (1990). A simple eddy kinetic energy model for simulations of the oceanic vertical mixing: Tests at station papa and long-term upper ocean study site. *Journal of Geophysical Research*, *95*(C9), 16179. doi: 10.1029/jc095ic09p16179

Gent, P. R., & McWilliams, J. C. (1990). Isopycnal mixing in ocean circulation models. *Journal of Physical Oceanography*, *20*(1), 150-155. doi: 10.1175/1520-0485(1990)020⟨0150:imiocm⟩2.0.co;2

Gordon, C., Cooper, C., Senior, C. A., Banks, H., Gregory, J. M., Johns, T. C., ... Wood, R. A. (2000). The simulation of SST, sea ice extents and ocean heat transports in a version of the Hadley Centre coupled model without flux adjustments. *Climate Dynamics*, *16*(2-3), 147-168. doi: 10.1007/s003820050010

Gregory, J. M. (2000). Vertical heat transports in the ocean and their effect on time-dependent climate change. *Climate Dynamics*, *16*(7), 501-515. doi: 10.1007/s003820000059

Gregory, J. M., Bouttes, N., Griffies, S. M., Haak, H., Hurlin, W. J., Jungclaus, J., ... Winton, M. (2016). The Flux-Anomaly-Forced Model Intercomparison Project (FAFMIP) contribution to CMIP6: investigation of sea-level and ocean climate change in response to CO2 forcing. *Geoscientific Model Development*, *9*(11), 3993-4017. doi: 10.5194/gmd-9-3993-2016

Griffies, S. (2012). *Elements of the modular ocean model (mom): 2012 release.* GFDL Ocean Group Tech. Rep. 7.

Griffies, S. M. (1998). The gent–McWilliams skew flux. *Journal of Physical Oceanography*, *28*(5), 831–841. doi: 10.1175/1520-0485(1998)028⟨0831:tgmsf⟩2.0.co;2

Huber, M. B., & Zanna, L. (2017). Drivers of uncertainty in simulated ocean circulation and heat uptake. *Geophysical Research Letters*, *44*(3), 1402-1413. doi: 10.1002/2016gl071587

Kraus, E. B., & Turner, J. S. (1967). A one-dimensional model of the seasonal thermocline II. The general theory and its consequences. *Tellus*, *19*(1), 98-106. doi: 10.1111/j.2153-3490.1967.tb01462.x

Kuhlbrodt, T., Gregory, J. M., & Shaffrey, L. C. (2015). A process-based analysis of ocean heat uptake in an AOGCM with an eddy-permitting ocean component. *Climate Dynamics*, *45*(11-12), 3205-3226. doi: 10.1007/s00382-015-2534-0

Large, W. G., McWilliams, J. C., & Doney, S. C. (1994). Oceanic vertical mixing: A review and a model with a nonlocal boundary layer parameterization. *Reviews of Geophysics*, *32*(4), 363. doi: 10.1029/94rg01872

Large, W. G., & Yeager, S. G. (2009). The global climatology of an interannually varying air–sea flux data set. *Climate Dynamics*, *33*(2-3), 341-364. doi: 10.1007/s00382-008-0441-3

Lowe, J. A., & Gregory, J. M. (2006). Understanding projections of sea level rise in a Hadley Centre coupled climate model. *Journal of Geophysical Research*, *111*(C11). doi: 10.1029/2005jc003421

Lyu, K., Zhang, X., Church, J. A., Slangen, A. B. A., & Hu, J. (2014). Time of emergence for regional sea-level change. *Nature Climate Change*, *4*(11), 1006-1010. doi: 10.1038/nclimate2397

Marshall, J., Adcroft, A., Hill, C., Perelman, L., & Heisey, C. (1997). A finite-volume, incompressible Navier Stokes model for studies of the ocean on parallel computers. *Journal of Geophysical Research: Oceans*, *102*(C3), 5753-5766. doi: 10.1029/96jc02775

Marshall, J., Scott, J. R., Armour, K. C., Campin, J.-M., Kelley, M., & Romanou, A. (2015). The ocean's role in the transient response of climate to abrupt greenhouse gas forcing. *Climate Dynamics*, *44*(7-8), 2287-2299. doi: 10.1007/s00382-014-2308-0

McDougall, T. J., & Barker, P. (2011). *Getting started with teos-10 and the gibbs seawater (gsw) oceanographic toolbox*. SCOR/IAPSO WG127.

Pardaens, A. K., Gregory, J. M., & Lowe, J. A. (2011). A model study of factors influencing projected changes in regional sea level over the twenty-first century. *Climate Dynamics*, *36*(9-10), 2015-2033. doi: 10.1007/s00382-009-0738-x

Saenko, O. A., Yang, D., & Gregory, J. M. (2018). Impact of mesoscale eddy transfer on heat uptake in an eddy-parameterizing ocean model. *Journal of Climate*, *31*(20), 8589-8606. doi: 10.1175/jcli-d-18-0186.1

Saenko, O. A., Yang, D., Gregory, J. M., Spence, P., & Myers, P. G. (2015). Separating the influence of projected changes in air temperature and wind on patterns of sea level change and ocean heat content. *Journal of Geophysical Research: Oceans*, *120*(8), 5749-5765. doi: 10.1002/2015jc010928

Simmons, H. L., Jayne, S. R., Laurent, L. C., & Weaver, A. J. (2004). Tidally driven mixing in a numerical model of the ocean general circulation. *Ocean Modelling*, *6*(3-4), 245-263. doi: 10.1016/s1463-5003(03)00011-8

Slangen, A. B. A., Carson, M., Katsman, C. A., van de Wal, R. S. W., Köhl, A., Vermeersen, L. L. A., & Stammer, D. (2014). Projecting twenty-first century regional sea-level changes. *Climatic Change*, *124*(1-2), 317-332. doi: 10.1007/s10584-014-1080-9

Swart, N. C., Cole, J. N. S., Kharin, V. V., Lazare, M., Scinocca, J. F., Gillett, N. P., … Winter, B. (2019). The canadian earth system model version 5 (CanESM5.0.3). *Geoscientific Model Development Discussions*, 1-68. doi: 10.5194/gmd-2019-177

Taylor, K. E., Stouffer, R. J., & Meehl, G. A. (2012). An Overview of CMIP5 and the Experiment Design. *Bulletin of the American Meteorological Society*, *93*(4), 485-498. doi: 10.1175/bams-d-11-00094.1

Tsujino, H., Urakawa, S., Nakano, H., Small, R. J., Kim, W. M., Yeager, S. G., … Yamazaki, D. (2018). JRA-55 based surface dataset for driving ocean–sea-ice models (JRA55-do). *Ocean Modelling*, *130*, 79-139. doi: 10.1016/j.ocemod.2018.07.002

Visbeck, M., Marshall, J., Haine, T., & Spall, M. (1997). Specification of eddy transfer coefficients in coarse-resolution ocean circulation models. *Journal of Physical Oceanography*, *27*(3), 381-402. doi: 10.1175/1520-0485(1997)027⟨0381:soetci⟩2.0.co;2

Wang, C., Zhang, L., Lee, S.-K., Wu, L., & Mechoso, C. R. (2014). A global perspective on CMIP5 climate model biases. *Nature Climate Change*, *4*(3), 201-205. doi: 10.1038/nclimate2118

Yang, D., & Saenko, O. A. (2012). Ocean Heat Transport and Its Projected Change in CanESM2. *Journal of Climate*, *25*(23), 8148-8163. doi: 10.1175/jcli-d-11-00715.1

Yin, J. (2012). Century to multi-century sea level rise projections from CMIP5 models. *Geophysical Research Letters*, *39*(17). doi: 10.1029/2012gl052947

Yin, J., Griffies, S. M., & Stouffer, R. J. (2010). Spatial Variability of Sea Level Rise in Twenty-First Century Projections. *Journal of Climate*, *23*(17), 4585-4607. doi: 10.1175/2010jcli3533.1

Zanna, L., Khatiwala, S., Gregory, J. M., Ison, J., & Heimbach, P. (2019). Global reconstruction of historical ocean heat storage and transport. *Proceedings of the National Academy of Sciences*, *116*(4), 1126-1131. doi: 10.1073/pnas.1808838115

Zika, J. D., Skliris, N., Blaker, A. T., Marsh, R., Nurser, A. J. G., & Josey, S. A. (2018). Improved estimates of water cycle change from ocean salinity: the key role of ocean warming. *Environmental Research Letters*, *13*(7), 074036. doi: 10.1088/1748-9326/aace42

Appendix A OGCM Parametrisations

As discussed in Section 2, all OGCMs used in this study employ the Gent and McWilliams (1990) parametrisation scheme to represent the effects sub-grid, mesoscale eddies. In the MOM cases (MOM5 and ACCESS-OM2), submesoscale eddy fluxes are parameterized following Fox-Kemper et al. (2008, 2011), and vertical mixing is performed using K-profile parameterisation (KPP) (Large et al., 1994). In NEMO3.4, momentum and tracers are vertically mixed using a turbulent kinetic energy (TKE) scheme based on the model of (Gaspar et al., 1990), with tidal mixing parameterised following Simmons et al. (2004). For HadOM3, the near surface vertical mixing is carried out via a Kraus-Turner mixed layer sub-model (Kraus & Turner, 1967).

In MITgcm and NEMO3.4, ocean temperatures are permitted to fall below freezing point, θ_{freeze}, but in the equation of state the temperature is constrained to be $\theta = \max(\theta, \theta_{freeze})$. In practice, global minimum annual mean temperatures remain above $-3°$C in the majority of experiments in these models. In HadOM3, if the ocean temperature falls below θ_{freeze}, it is reset to θ_{freeze}, with the associated heating coming from a cooling of the layer immediately beneath. If a flux perturbation causes the whole water column to freeze, the remaining negative heat flux is lost from the system.

Table 1. Ocean GCMs and coupled, atmosphere-ocean GCMs used in this study.

General Circulation Model	Grid (latitude $\times$ longitude)	Time step (hours)	Spin up data	Citation
Massachusetts Institute of Technology general circulation model, checkpoint 66o (MITgcm)	$2.8° \times 2.8°$ and 15 z levels	12 h	Time mean CanESM2 (Chylek et al., 2011) pre-industrial control (piControl, (Taylor et al., 2012)) following (Huber & Zanna, 2017). SST and SSS relaxation at 60 and 90 days, respectively.	Marshall et al. (1997)
NOAA-GFDL Modular Ocean Model, version 5 (MOM5)	nominally $1° \times 1°$ and 50 z^* levels	2 h	CORE version 2 (Large & Yeager, 2009)	S. Griffies (2012)
Ocean-sea ice component of the Australian Community Climate and Earth System Simulator (ACCESS-OM2)	nominally $1° \times 1°$ and 50 z^* levels	2 h	JRA55-do normal year forcing (Tsujino et al., 2018), SST and SSS relaxation at 30 and 60 days, respectively.	S. Griffies (2012)
Nucleus for European Modelling of the Ocean, version 3.4 (NEMO3.4)	nominally $1° \times 1°$ (ORCA1 C-grid) and 45 z levels	1 h	Pre-industrial CanESM2 control (Yang & Saenko, 2012)	Swart et al. (2019), Saenko et al. (2018)
Hadley Centre Ocean Model, version 3 (HadOM3)	$1.25° \times 1.25°$ and 20 z levels	1 h	Pre-industrial	Gordon et al. (2000)
Candian Earth System Model, version 5 (CanESM5)	ocean: NEMO3.4 atmosphere: nominally $2.8° \times 2.8°$ (T63 spectral resolution) 49 hybrid vertical levels to 1 hPa	ocean: 1 h coupler: 3 h	Pre-industrial	Swart et al. (2019)
Hadley Centre Climate Model, version 3 (HadCM3)	ocean: see HadOM3 atmosphere: $2.5° \times 3.75°$ and 19 vertical levels	ocean: 1 h coupler: 24 h	Pre-industrial	Gordon et al. (2000)